Merits and Limits of SWAT-GL: Application in Contrasting Glaciated Catchments

Timo Schaffhauser[1], Florentin Hofmeister[1,2], Gabriele Chiogna[3], Fabian Merk[1], Ye Tuo[1], Julian Machnitzke[1], Lucas Alcamo[1], Jingshui Huang[1], and Markus Disse[1]

[1]School of Engineering and Design, Technical University of Munich, Munich, Germany
[2]Bavarian Academy of Sciences and Humanities, Munich, Germany
[3]GeoZentrum Norbayern, Friedrich-Alexander-Universität Erlangen-Nürnberg (FAU), Erlangen, Germany

Correspondence: Timo Schaffhauser (t.schaffhauser@tum.de)

Abstract. The recently released SWAT-GL aims to overcome multiple limitations of the traditional hydrological model SWAT (Soil Water Assessment Tool) in glaciated mountainous catchments. SWAT-GL intends to increase the applicability of SWAT in these catchments and to reduce misapplication when glaciers have a significant role in the catchment hydrology. It thereby relies on a mass balance module, based on a degree-day approach similar to SWAT's snow melt module, extended by a glacier

5 evolution component which is based on the delta-h (Δh) parameterization. The latter one is a mass conserving approach which enables the spatial distribution of ice thickness changes and thus dynamic glacier retreat. However, the extended SWAT version was not yet comprehensively benchmarked. Hence, our paper aims to evaluate SWAT-GL with four different benchmark glaciers, which are part of the USGS (United States Geological Survey) Benchmark Glacier Project. The benchmarking considers a comprehensive evaluation procedure, where SWAT-GL is optimized on glacier mass balance and hypsometry as well

10 as snow cover. Snow cover is included to consider snow-glacier feedbacks. Besides, a sensitivity analysis using Elementary Effects (or Method of Morris) is performed to give a detailed picture on the importance of the introduced glacier processes, as well as the relevance of the interactions with the already-existing snow routine. We intentionally did not include discharge in the optimization procedure to fully demonstrate the capabilities of SWAT-GL in terms of glacier and snow processes. Results demonstrate that SWAT-GL is able to represent the characteristics of contrasting glaciated catchments, which underlines

15 SWAT-GL's applicability and transferability. We could further show its strong (non-linear) interactions with the existing snow routine suggesting a simultaneous calibration of the snow components. While snow and glacier processes were adequately represented in the catchments, discharge was not necessarily represented sufficiently when excluded in the optimization procedure. However, SWAT-GL has been shown to be easily capable of reproducing discharge when used in a stand-alone optimization, although this may come at the expense of model consistency. Lastly, SWAT-GL significantly outperformed a standard SWAT

20 model used for benchmarking purposes in high mountain environments.

1 Introduction

We recently submitted a paper that introduces a new glacier routine to the Soil Water Assessment Tool (SWAT) to overcome current limitations in its applicability, especially in glaciated catchments (Schaffhauser et al., 2024). The work is built on pre-

vious efforts of multiple groups which intend to address common constraints of conceptual and physically-based hydrological
models in glacier-dominated catchments. Examples include the work of Seibert et al. (2018) or Li et al. (2015) for HBV (Hydrologiska Byråns Vattenbalansavdelning), Wortmann et al. (2016) for SWIM (Soil and Water Integrated Model) or Shannon et al. (2022) for the DECIPHeR model (Dynamic fluxEs and ConnectIvity for Predictions of HydRology). However, to our knowledge many hydrological models do not include glacier routines by default and glacier-focused extensions are often only available to the developing groups, although trends are clearly towards publishing model code and making it openly accessible. Despite these improvements, applications in glaciated basins remain challenging due to missing (or very simple) glacier representations, whereby modelers might rely on external couplings of glaciological and hydrological models (Adnan et al., 2019; Wu et al., 2015; Stoll et al., 2020; Du et al., 2022; Naz et al., 2014; Wiersma et al., 2022; Chen et al., 2017). As it is commonly known, glacio-hydrological models applied to small and highly glacierized catchments often have no or a rather rough representation of additional hydrological components (e.g., evapotranspiration) (Hassan et al., 2021; Ali et al., 2017; Pradhananga et al., 2014), potentially leading to an integration problem, at least when the model domain is extended (Tiel et al., 2020; Wortmann et al., 2016). A further problem is that it is not always clear in the existing literature whether, for example, a glacier routine is coupled with or integrated into an hydrological model, if this hydrological model by default does not take glacier processes into account (e.g., SWAT, VIC—Variable Infiltration Capacity—, HBV) and is used to simulate glacio-hydrological processes. The terms *integrated* and *coupled* seem to be used interchangeably, thus impairing reproducibility. From our perspective, integration should suggests a model expansion, while coupling suggests the use of an additional model. Besides, distinctions are not always easy and clear especially what coupling exactly means. In our understanding, coupling usually refers to a chained approach, where external information, e.g. from a snow module, are used as input for a hydrological model without an exchange of information of the two.

Depending on the research question and data available, several glacier routines with different complexity are available for simulating glacier mass balances and melt contribution in hydrological models. An unlimited ice storage that generates melt water based on a calibrated degree-day factor represents the simplest empirical routine (Naz et al., 2014). However, this routine cannot consider glacier evolution, such as glacier retreat. Conceptual routines, such as the volume-area scaling (VA scaling) (Bahr et al., 2015) or the Δh-parameterization (Huss et al., 2010), simulate the spatial dynamic of a glacier as a simplified function of glacier extent, thickness, and elevation range (Tiel et al., 2020). The largest limitation of these methods is the lack of an actual representation of the ice flow dynamic, which can be simulated with full physics-based algorithms (Zekollari et al., 2022). Since ice flow modules require several input data and the definition of distinctive boundary conditions, such as bedrock roughness, the application is usually beyond the scope of common water balance simulations in glaciated catchments. In recent years, the coupling of water balance simulation models with global glacier models has proven to be a valuable method for predicting the hydrological response of catchments in mountainous regions under a changing climate (Pesci et al., 2023).

Past SWAT-specific efforts to improve capabilities in glacier-fed catchments other than those from Schaffhauser et al. (2024) for example refer to the work of Luo et al. (2013), who implemented a VA scaling for glacier evolution along with a degree-day-based mass balance module. The modified SWAT version was further applied in several studies, mostly focusing on China (Gan et al., 2015; Luo et al., 2018; Ma et al., 2015; Shafeeque et al., 2019; Wang et al., 2018) and recently integrated in

SWAT+ (Yang et al., 2022). However, to the best of our knowledge in none of the publications the model code was made
publicly available. Besides, Ji et al. (2019) for instance implemented an ice melt routine based on a degree-day approach but
did not account for glacier evolution explicitly. Unfortunately, none of the approaches was included in any of the official SWAT
revisions. SWAT-GL was developed to tackle these issues and to provide a freely available and user-friendly SWAT version for
glaciated catchments (Schaffhauser et al., 2024). Besides, the chosen approach, namely the Δh-parameterization from Huss
et al. (2010) has proven to be a robust method to simulate glacier evolution in glaciated catchments (Huss and Hock, 2015).

However, no comprehensive evaluation of SWAT-GL has been conducted to date. As glaciers and high-mountainous catchments
are usually rather data-scarce (Tuo et al., 2016), testing the performance of glacio-hydrological models for long observed time
series of good quality is challenging. Moreover, in many cases the available variables to calibrate and validate the model are
limited to discharge only, with these gauges often located much further downstream and not close to the glacier. Evaluating
the glaciological routines of glacio-hydrological models by discharge alone, representing a superposition of multiple signals,
might be problematic, as it might not reflect the signatures which would be visible in the glaciological components. In other
words, a satisfactory representation of discharge used to evaluate catchment glaciology (or other processes), albeit often done,
might be inadequate. Nevertheless, a sound evaluation of newly introduced schemes in glacio-hydrological models (e.g., glacier
components into a hydrological model) should be desired and aimed for. If a mass balance module is implemented together
with an evolution module (as in SWAT-GL), in the best case both are evaluated individually and complemented by discharge
assessments.

The USGS Benchmark Glacier Project (O'Neel et al., 2019) is a promising attempt to overcome current limitations in data
accessibility and modeling efforts of high-mountainous and glaciated basins. The project involves five glaciers, four where
long-term measurements are available and one for which the project expanded more recently. The glaciers, namely Gulkana,
Wolverine, Lemon Creek, South Cascade and Sperry Glaciers, are located across the Northern United States and thus charac-
terized by various climate regimes (O'Neel et al., 2014; O'Neel et al., 2019). As each glacier is situated within the catchment
of a close-by discharge gauge, they are well-suited for glacio-hydrological studies. Long-term hydrological, meteorological,
glaciological as well as geodetic measurement are available for each glacier, which range back to the 1950s in terms of mass
balance and glacier area observations. O'Neel et al. (2019) found that mass loss is not only present from the beginning of the
measurements but has actually increased for four of the five glaciers since the 1990s. A trend which is likely to continue under
global temperature projections (Tebaldi et al., 2021).

This paper evaluates the recently developed SWAT-GL model with a focus on its novel glaciological components. A sensitiv-
ity analysis (SA) using the method of Morris (Morris, 1991), also known as Elementary Effects (EE), is conducted to screen
and rank the new input factors under different conditions. Additionally, the model is assessed against long-term glacier mass
balance and glacier area-altitude (hypsometry) measurements. Given the interactions between the snow and glacier routines,
the evaluation also considers the model's ability to simulate snow cover. Discharge is used for cross-validation under the hy-
pothesis that a well-performing snow and glacier routine in alpine catchments is sufficient to reproduce discharge. Lastly,
the performance of the snow- and glacier-optimized SWAT-GL model is compared to a discharge-only optimized and a mass
balance-only optimized SWAT-GL model, as well as two standard SWAT models that serve as upper and lower benchmarks

without considering glacier processes. The evaluation is performed for four highly glaciated catchments across the US based

95   on the USGS Benchmark Glacier Project (O'Neel et al., 2019).

2   Materials & Methods

In the following we will briefly introduce the USGS Benchmark Glacier Project, the chosen datasets for the evaluation, the study area as well as the evaluation and sensitivity analysis approach.

2.1   Datasets & USGS Benchmark Glacier Project

100   The study is based on the USGS Benchmark Glacier Project (O'Neel et al., 2019) which provides data for five long-term monitoring glaciers across the Northern United States (Mcneil et al., 2016; Baker et al., 2018). The five sites are distributed over Alaska, Washington and Montana and thus represent coastal as well as inland locations. Long-term meteorological, geodetic and glaciological measurements starting from the 1950s or 1960s onward are available for four of the glaciers. For the relatively new Sperry Glacier in the program only short time series (from 2005 on) are available: therefore it was excluded in this

105   study. In the following we only refer to the Gulkana (GG), Wolverine (WG), South Cascade (SCG) and Lemon Creek (LCG) glaciers. Seasonal mass balance estimates are derived from geodetically calibrated, conventional glacier-wide mass balance observations (Mcneil et al., 2016). The project combines measurements with homogeneous data processing methods to allow for inter-glacier comparisons. An overview of the acquisition years of the geodetic surveys can be found in O'Neel et al. (2019). Glaciological field visits of each glacier take place every spring and fall. Summarizing, the following glaciological variables

110   were used from the USGS Glacier Benchmark Project, total annual glacier area (km^2), annual net mass balance change (m w.e.), annual glacier hypsometry (km^2 at a specific elevation range) (see Table 1). Glacier hypsometries hereby represent the area-altitude distribution of the glacier.

Continuous daily meteorological time series (precipitation & temperature) are directly available on-site for the GG & WG. However, although on-site measurements are also available for the LCG & SCG, the time series are rather short and show a

115   relatively high amount of missing values. For reasons of comparability we follow the approach of O'Neel et al. (2019) and use the closest representative station, which is Juneau Airport (LCG) and Diablo Dam (SCG), respectively. The latter two are also part of the official data of the USGS Benchmark Glacier Project (Baker et al., 2018).

However, since SWAT-GL needs minimum daily (T_{min}) and maximum daily temperature (T_{max}) which was not continuously available in the project for GG (starting 1995) and WG (starting 1997), a regression model was established to produce continu-

120   ous daily T_{min} and T_{max} time series. In detail, daily mean temperature was used as predictor of either T_{max} or T_{min} in the period where all three variables were available. Subsequently, the regression model was used to predict T_{max} and T_{min} backwards for the periods before 1995 (GG) and 1997 (WG), respectively. Data gaps of up to three days were linearly interpolated and longer gaps were regressed using daily data from the closest meteorological station of each glacier. The approach is similar to O'Neel et al. (2019), with the only difference that they used monthly regression for longer gaps. We also investigated the potential

125   of the ERA5-Land (Copernicus Climate Change Service, 2019) data to fill gaps, which was inadequate, especially due to a significant precipitation bias throughout the annual cycle and between years, compared to the station data (see Fig. A1).

Hydrological data was obtained from the USGS National Water Information System (U.S. Geological Survey, 1994). We used

Table 1. Overview of datasets used. P represents precipitation (mm), T temperature (°C), Q discharge (m^3/s) and SC snow cover (%). Glaciological data is a merged representation of annual net mass balance change (B_{gl} in m w.e.), total annual glacier area (A_{gl} in km^2) and annual glacier hypsometry (H_{gl} in km^2 at a specific elevation range). *var.* indicates that measurements stem from various locations or refer to the whole glacier. The elevation in the glaciological dataset section refers to the total glacier elevation range.

Glacier Basin	Site	Variable	Time Step	Lat	Lon	Elevation [masl]	Temporal Coverage	Missing [%]
Meteorological								
GG	On-site	P	Daily	63.26	-145.41	1,480	1964-2022	9
		T						12
WG	On-site	P	Daily	60.39	-148.94	990	1964-2022	12
		T						14
LCG	Juneau Airport	P	Daily	58.35	-134.56	6	1936-2022	<1
		T						<1
SCG	Diablo Dam	P	Daily	48.71	-121.14	272	1914-2022	<1
		T						<1
Hydrological								
GG	Phelan Creek	Q	Daily	63.24	-145.47	1,127	1966-2023	19
WG	Wolverine Creek	Q	Daily	60.37	-148.9	366	1964-2023	57
LCG	Lemon Creek	Q	Daily	58.39	-134.42	204	1951-2023	41
SCG	SF Cascade	Q	Daily	48.37	-121.07	1,613	1957-1993	28
Snow								
All Basins	Basin mean	SC	Monthly	-	-	-	2002-2023	0
Glaciological								
GG	On-site	B_{gl}	Annual	*var.*	*var.*	1,185-	1966-2022	0
		A_{gl}				2,420	1965-2022	0
		H_{gl}						0
WG	On-site	B_{gl}	Annual	*var.*	*var.*	466-	1966-2022	0
		A_{gl}				1,653	1965-2022	0
		H_{gl}						0
LCG	On-site	B_{gl}	Annual	*var.*	*var.*	543-	1953-2022	0
		A_{gl}				1,550	1946-2022	0
		H_{gl}						0
SCG	On-site	B_{gl}	Annual	*var.*	*var.*	1,619-	1959-2022	0
		A_{gl}				2,439	1950-2022	0
		H_{gl}						0

the closest available gauge for each glacier to determine the total basin area. In detail, the discharge data of the Phelan Creek (representing the GG basin), Wolverine Creek (WG basin), Lemon Creek (LCG basin) and the SF Cascade (SCG basin) was used. Details about the meteorological and hydrological sites and time series are found in Table 1.

130

Snow cover (SC) data was derived from the MOD10A1 & MYD10A1 V061 NDSI (Normalized Difference Snow Index) products with 500 m resolution. The NDSI is based on optical sensors from MODIS (Moderate Resolution Imaging Spectroradiometer) and is calculated as the difference between the reflection in the green spectrum (GREEN) and the short-wave infrared (SWIR) divided by the sum of the two (Dozier, 1989).

$$I_{NDSI} = \frac{B_{GREEN} - B_{SWIR}}{B_{GREEN} + B_{SWIR}} \tag{1}$$

where I_{NDSI} is the NDSI and B_{GREEN} and B_{SWIR} are the green and SWIR bands, respectively.

For the classification of snow or no-snow pixels a NDSI threshold of 0.4 was used, where values above 0.4 (Hofmeister et al., 2022) indicate snow pixels and smaller values are classified as snow-free. Daily fractional SC (%) on the basin and subbasin scale was then calculated as the average of snow-covered pixels within each basin. Subsequently monthly aggregates were produced. MODIS NDSI data was available from 2002 up to now. A full overview of all datasets is given in Table 1. Auxiliary datasets used were elevation data from the Shuttle Radar Topography Mission (SRTM) (NASA JPL, 2013), the Randolph Glacier Inventory V6 (RGI) (RGI Consortium, 2017) as well as ice thickness estimates from Farinotti et al. (2019).

2.2 Study Area

The location of the USGS Benchmark Glaciers combined with the location of the corresponding hydrological and meteorological stations used for each glacier is shown in Fig. 1. Note that the representative meteorological stations which were used to force the SWAT-GL models of the SCG and LCG are not shown as they are situated outside of the basin boundaries (see O'Neel et al. (2019) for more details). Besides, the map contains the basin boundaries for each glacier which were used as model domain. The total glacier area in each catchment is slightly higher than the individual glacier area of each glacier, as the basins can include several adjacent glaciers. However, the main glacier fraction can be accounted to the four benchmark glaciers in each basin.

The basins have an area of 28.4 km^2 (GG, 64% glaciated 2009), 23.9 km^2 (WG, 69% glaciated 2006), 29.3 km^2 (LCG, 50% glaciated 2005) and 5.9 km^2 (SCG, 58% glaciated 1958). Basin-wide glacier fractions were determined using Randolph Glacier Inventory data (RGI Consortium, 2017). Each glacier hereby represents a distinct climate regime, where the most northward located GG is characterized by a continental (high-latitude) climate (O'Neel et al., 2014; O'Neel et al., 2019). WG, in contrast, is characterized by a maritime (high-latitude) climate regime (O'Neel et al., 2014; O'Neel et al., 2019). LCG represents another high-latitude maritime glacier, while SCG represents a mid-latitude maritime glacier (O'Neel et al., 2019; Horlings, 2016). All glaciers are retreating, where the SCG shows the strongest relative recession with a glacier area loss of more than 40% (1.3 km^2) since 1950. GG lost around 18% (3.3 km^2) of its area since 1965, LCG decreased by 16% (3.3 km^2) from 1946 up to now and WG receded around 12% (2 km^2) compared to 1965. Glacier recession magnitudes reveal a gradient from North to South (O'Neel et al., 2019). Mass balance rates are provided in Fig. 3, which show an increasing negative (statistically significant) trend at all sites (O'Neel et al., 2019). According to O'Neel et al. (2019) total uncertainty, consisting of a geodetic and glaciological component, in the mass balance estimates is around 0.2 m w.e. a^{-1} except for GG where it is higher with 0.4 m w.e. a^{-1}.

The following mean climate characteristics of each basin were evaluated based on the meteorological stations listed in Table
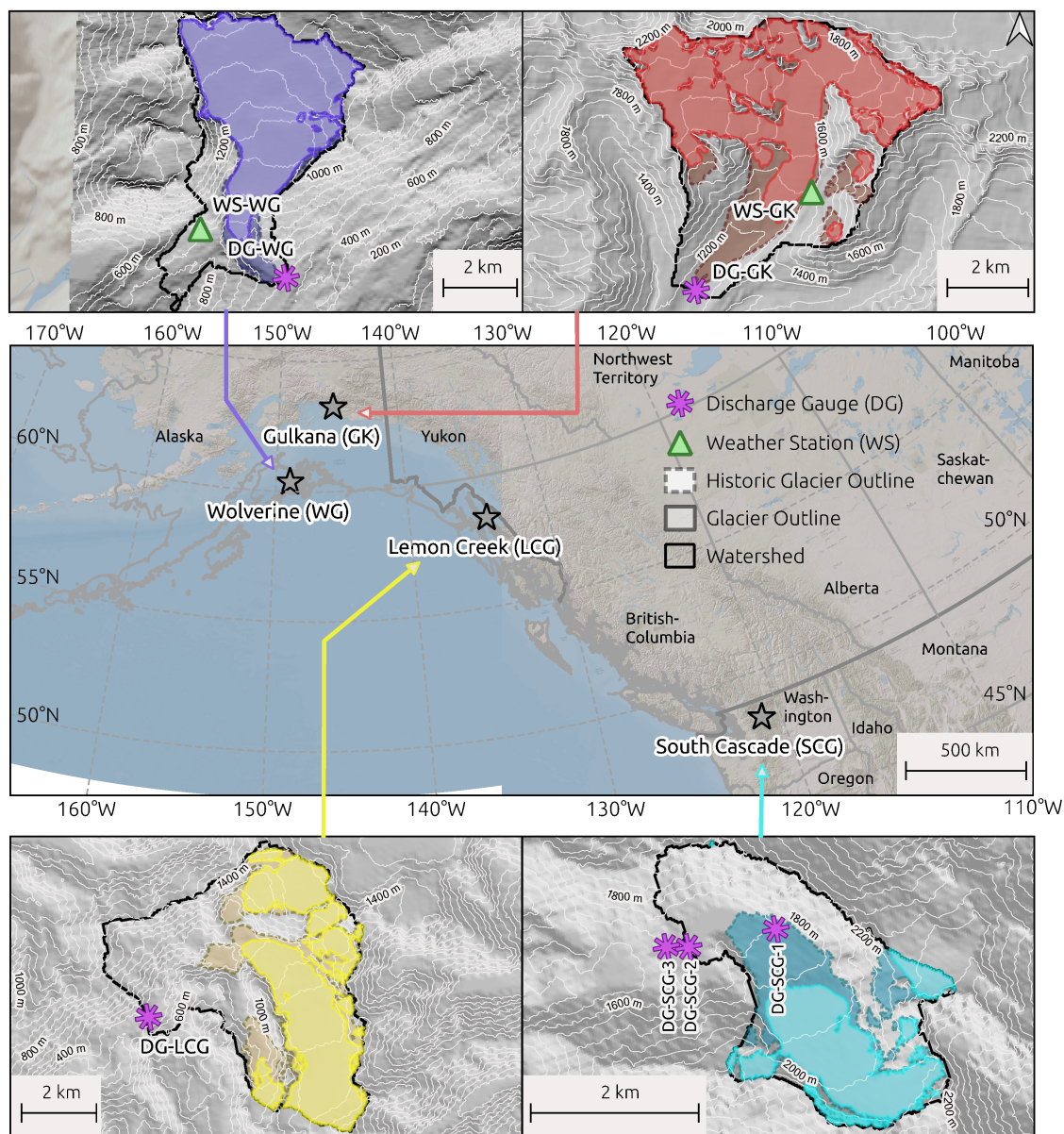
Figure 1. Overview of the four USGS Benchmark Glaciers used in this study. Note that the SCG & LCG meteorological stations that were used are remote stations which is why they are not visible in the map. The transparent outline refers to a historical date, the filled outline to a recent date. The dates are: 1957/2021 GG, 1950/2020 WG, 1948/2021 LCG, 1958/2021 SCG.

165   1 and the period 1971-2000. The continental GG with an annual average precipitation of ~1,480 mm and a peak in August/
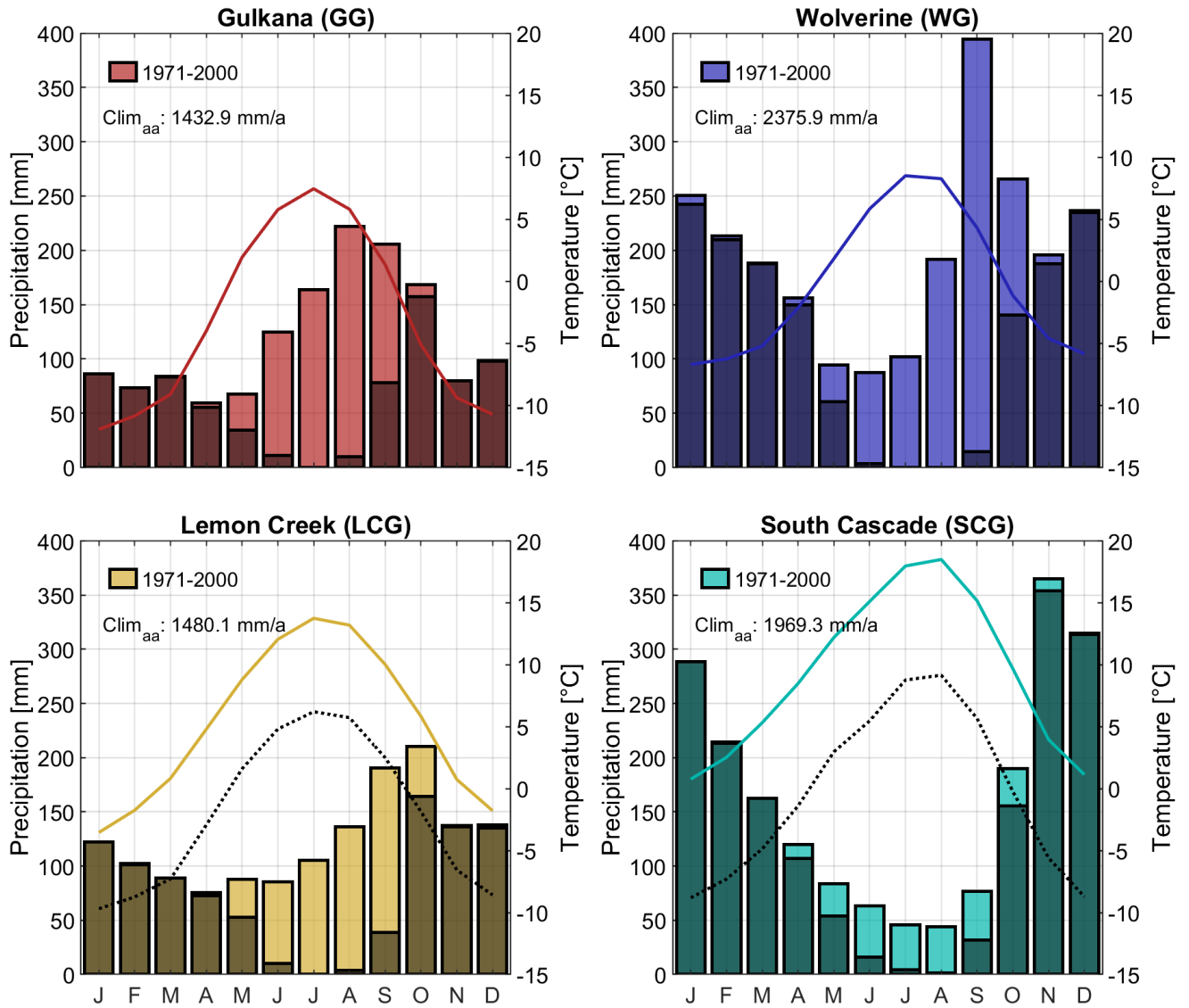
Figure 2. Overview of the mean climate regimes of the four glaciers according to the stations of Table 1 and the reference period 1971-2000. Lines refer to monthly mean temperatures and bars to mean monthly precipitation sums. As the LCG and SCG stations are remote and lower-elevated (20 and 40 km apart and at 6 m and 270 m), black dotted lines representing temperature based on a -6.5 °C/km lapse rate were provided additionally. The letters from J to D correspond to the months January to December. $Clim_{aa}$ refers to the annual average precipitation for the indicated periods. Black overlapping bars represent a solid precipitation proxy assuming that snowfall occurs when temperature is below 1 °C.

September is significantly drier than its maritime counterparts. SCG with an annual average of 1,970 mm and WG with an annual mean of 2,375 mm show the highest precipitation values among the four. While WG has its precipitation peak roughly in September/ October it also shows consistent high precipitation during the Winter months and a dry period in summer. SCG is also characterized by a summer low, followed by an increase in precipitation during Autumn and ending in a strong late Autumn and Winter peak (November - January). The annual precipitation totals of the LCG are around 1,480 mm with a less pronounced peak in Autumn. The glacier generally has a lower gradient between wet and dry period, which makes precipitation more evenly distributed throughout the year. In terms of temperatures, all glaciers reach their maximum in either July or August and their yearly minimum in January. The mean climates are illustrated in Figure 2. However, it should be noted that no lapse rates have been applied for the climate classification, the meteorological station used for LCG and SCG come with an elevation difference of more than 500-1,500 m (LCG) and 1,300-2,100 m (SCG). Lapse rates (temperature and precipitation) were later calibrated through the optimization procedure (see section 3.3).

All gauges belong to intermittent streams, which can fall dry during the winter months (Fig. 3). While the corresponding streams of GG and WG had almost no flow in the available time series (see Table 1) from December to April/May, the streams of SCG and LCG carried water sporadically during these months. Annual average flows are 2.4 m³/s (GG), 2.7 m³/s (WG), 5.5 m³/s (LCG), 28.1 m³/s (SCG) evaluated for the period 2002-2022 for all glaciers except SCG, where the years from 1972-1992 had to be chosen (due to a lack of observations). Inter-annual variability is highest at GG (Coefficient of Variation—CV—of 0.21) and lowest at SCG (CV of 0.13). Except for the SCG basin, we can see a tendency of a slight shift in the flow period towards an earlier onset of the melt season (Fig. 3).

2.3 SWAT-GL

The recently developed SWAT-GL (Schaffhauser et al., 2024) is a modified version of the traditional hydrological model SWAT (Arnold et al., 1998), which includes glacier dynamics based on the Δh approach developed by Huss et al. (2010). The empirical Δh-parameterization is called annually to translate the cumulative mass balance change to a change in glacier geometry. The concept assumes that lower elevated areas closer to the glacier terminus receive stronger ablation than higher elevated ones (Huss et al., 2008, 2010). Therefore, glaciers are divided into different elevation sections (ES) for the application. In addition to its spatial distributed applicability the method is mass-conserving and can be applied with glacier outlines and glacier thickness data only (Li et al., 2015; Seibert et al., 2018).

It basically consists of two modules, a mass balance and a glacier evolution module. Mass balance estimations are based on a degree-day approach, similar to the already existing snow routine of SWAT. Glacier evolution is implemented by means of the Δh approach (Huss et al., 2008, 2010). For detailed technical explanations we refer to Schaffhauser et al. (2024), as we only provide a short summary of the main points here.

In general, the mass balance is formulated as:

$$W_t = W_{t-1} - M_t \cdot (1 - \beta_f) - S_t + C_t \tag{2}$$
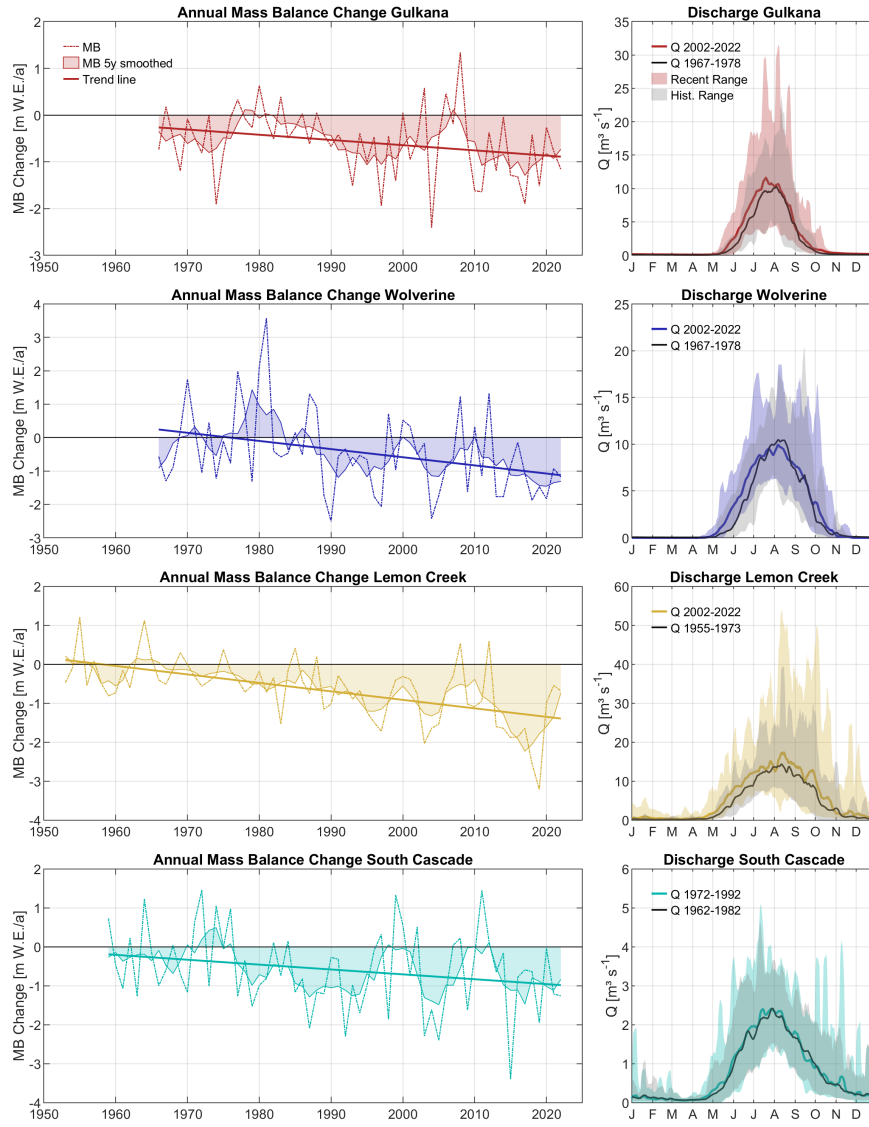
Figure 3. Overview of the annual mass balance rates of all glaciers merged with the mean daily discharge of two periods for each glacier. The recent periods refer to 2002-2022 (GG, WG, LCG) and 1972-1992 (LCG) and the older periods refer to 1967-1978 (GG, WG), 1955-1973 (LCG) and 1962-1982 (SCG) as indicated in the day of the year plots.

with W_t being the water equivalent of ice [mm $H_2O \cdot d^{-1}$] at day t, M_t represents the melt rate [mm $H_2O \cdot d^{-1}$], S_t represents the sublimation rate [mm $H_2O \cdot d^{-1}$], C_t refers to the accumulation rate [mm $H_2O \cdot d^{-1}$] and β_f is an adjustable refreezing factor of ice during melt periods. M_t is calculated analogously to snow melt in the standard SWAT using a distinct melt factor.

The physically-based Δh-parameterization is able to simulate spatially distributed glacier retreat. The core of the approach is that glaciers are discretized in elevation sections, where each has an inherent storage and receives distinct ice thickness changes. The ES are normalized for the glacier elevation range and a characteristic (normalized) ice thickness change is assigned to each zone, according to:

$$E_{norm,i} = \frac{E_{max} - E_i}{E_{max} - E_{min}} \tag{3}$$

where $E_{norm,i}$ is the normalized elevation of ES i [-], E_{max} and E_{min} refer to the maximum and minimum glacier elevation [m], and E_i is the actual elevation of ES i [m].

Lower altitudes hereby receive stronger ablation than higher ones. The characteristic ice thickness change for each normalized elevation varies with glacier size. One of three parameterizations is used separately for each glacier, which are thus classified as small (<5 km^2), medium (5-20 km^2) or large (>20 km^2). The empirical relationship is illustrated in Fig. 4. It is important to note that the Δh-parameterization is called annually (at the end of a glaciological year) to redistribute (lumped) annual mass balance changes over the individual ES of a subbasin to simulate glacier retreat. The normalized ice thickness change formulas of Fig. 4 follows the general form

$$\Delta h_i = (E_{norm,i} + a)^y + b \cdot (E_{norm,i} + a) + c \tag{4}$$

where a, b, c, y are coefficients which vary for glacier size and Δh_i represents the normalized ice thickness change for an Elevation E_i. We use the parameters based on Huss et al. (2010). Theoretically the parameters could be derived specifically for any glacier if the required data is available (e.g. two DEMs at different dates). The dimensionless ice thickness change Δh_i is rescaled using a scaling factor f_s [m] to receive the change in meters for every glaciological year (5).

$$f_s = \frac{V_a}{\sum_{i=1}^{n} A_i \cdot \Delta h_i} \tag{5}$$

with V_a referring to the annual glacier volume change expressed in water equivalent [m^3], that is calculated by multiplication of annual EW values (see Eq. 2) and the subbasin area. A_i is the area of ES i with n being the total number of ES. Annual ice thickness changes are then calculated via

$$h_{i,1} = h_{i,0} + f_s \cdot \Delta h_i \tag{6}$$

where $h_{i,1}$ is the updated ice thickness [m water equivalent] after each glaciological year of ES i, $h_{i,0}$ is the ice thickness [m water equivalent] in ES i before the application of Δh parameterization. If $h_{i,1}$ is ≤ 0 the ES is assumed ice-free causing an update of the glacier extent.

SWAT-GL classifies glaciers on the subbasin scale, meaning that a simplified assumption is used where all glaciated areas within a subbasin are considered as one glacier object. The implementation of the glacier routine in SWAT introduces five new parameters which control glacier melt (and refreezing) and accumulation. Besides, one new output file containing annual glacier mass balance information (for each glaciological year) as well as two new input files which require some preprocessing

are introduced. The two input files refer to the parameterization on the HRU scale as well as the glacier initialization with respect to hypsometry, ice thickness and volume. The source code of SWAT-GL together with an example is freely accessible via GitLab https://gitlab.com/lshm1/swat-g.
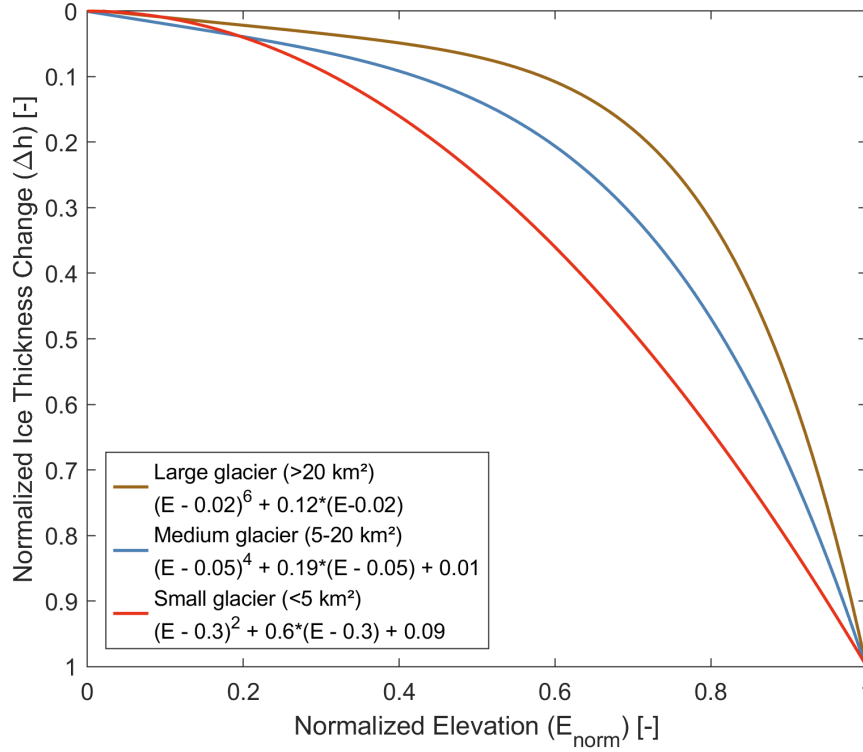
Figure 4. Empirical relationship of normalized glacier elevation and the normalized ice thickness change based on Huss et al. (2010).

2.4 Sensitivity Analysis

235   In order to provide a comprehensive picture of SWAT-GL we also performed a global sensitivity analysis using the Method of Morris or Elementary Effects (Morris, 1991; Saltelli et al., 2008). The method which is based on a multiple-starts perturbation approach and thus belongs to the one at a time (OAT) methods is able to determine approximate sensitivities at a relatively low computational cost (Saltelli et al., 2008; Pianosi et al., 2016). A lower computational cost hereby refers to the fact that the total number of simulations required is significantly reduced compared to other methods, such as for the Sobol method. The EEs

240   test has thus been established as a robust method for screening and ranking of the input factors (Pianosi et al., 2016).

    For sampling we used the radial design, where r sample points from a Latin hypercube sampling serve as well-spread starting points in the input space (Campolongo et al., 2011). The total sample size N follows the form $r(M + 1)$, with M being the number of input factors. For r a value of 500 was chosen, resulting in 7,500 model evaluations ($M = 14$) (Sarrazin et al.,

2016). A value of r=500 can be considered as sufficient for screening and ranking purposes, for example Vanuytrecht et al.
(2014) has shown that a stable ranking was achieved using only 25 trajectories, whereby the relatively small numbers of simulations necessary for ranking was further confirmed by Nossent et al. (2011). The basic idea of the radial design is that from a starting point, one factor M is varied while keeping all others fixed. This results in M steps (varying each factor once) that are performed for each sampling point (r). In general, r EEs are calculated per input factor which are then averaged to provide a global sensitivity metric μ_i for each input factor i. The calculation itself is based on finite differences. To account for non-monotonic effects in the model, μ_i^* is used based on the absolute values of the EEs (Campolongo et al., 2011). The formulation is:

$$\mu_i^* = \frac{\sum_{i=1}^{r} |\mathrm{I}_{EE,i}|}{r} \tag{7}$$

An EE of an input factor i can be calculated as follows:

$$\mathrm{I}_{EE,i} = \frac{Y(X_1, X_2, ..., X_{i-1}, X_i + \Delta, ..., X_M) - Y(X_1, X_2, ..., X_M)}{\Delta} \tag{8}$$

with $I_{EE,i}$ being an elementary effect of input factor i and $X = (X_1, X_2, ..., X_M)$ being the individual values of the factors and Δ the step (or perturbation). We also calculated the standard deviation σ_i of the EEs as a proxy of the interaction of input factor i with the other factors. It also describes whether the model output is linearly or non-linearly affected by an input factor (Garcia Sanchez et al., 2014; Merchán-Rivera et al., 2022). To avoid confusion with other sigmas used in this work, we define sigma of an EE as $\sigma_{EE,i}$. The ratio of $\sigma_{EE,i}/\mu_i^*$ also provides insights into whether the effect of a factor is monotonous or almost monotonous as explained in Garcia Sanchez et al. (2014); Merchán-Rivera et al. (2022). This is especially important to derive information whether the interaction of snow and glacier processes are represented (adequately). Due to the different scales of the input factors, the standardization of Sin and Gernaey (2009) was applied. The SA is used to support and complement the benchmarking procedure to i) determine the importance of the newly introduced parameters under different conditions, ii) rank the parameters to get insights into how the most influential parameters differ between the catchments and iii) identify whether the glacier routine interacts appropriately with the snow routine. For the SA the combined calibration period from 2002-2015 and validation period from 2016-2022 was used.

2.5 SWAT-GL Testing Methodology

The core of the study is to evaluate the capabilities of SWAT-GL to simulate multiple glaciological components in glaciated catchments. This involves the assessment of SWAT-GL based on he representation of multiple snow and glacier variables in the four glaciated catchments. The glacier and snow optimized SWAT-GL model is further compared with a discharge only and mass balance only optimized SWAT-GL model. Lastly, two SWAT standard models are introduced that do not consider glacier processes and serve as upper and lower benchmark estimates in comparison to SWAT-GL.

2.5.1 Preprocessing & Initialization

275 SWAT-GL needs distributed glacier thickness and glacier area information as input for each ES and subbasin. However, this data is usually not easily available for various years. In most cases, only globally and openly available datasets such as glacier areas from the RGI (RGI Consortium, 2017) and ice thickness from Farinotti et al. (2019) or Millan et al. (2022), representing a fixed point in time, are available to use. Alternatively, if geodetic information is available at different times, glacier thickness can also be directly inferred for each of them. As the USGS Benchmark glacier project provides geodetic data for several years

280 we have chosen the best available DEM closest to the mass balance observation start of each glacier. Best hereby refers to a full coverage of the glacier basins along with a minimum of missing values. The thickness was then estimated using the GlabTob2 model (Linsbauer, A et al., 2009; Linsbauer et al., 2012; Frey et al., 2014). Glacier outlines were also available at several times in the Benchmark project and the year closest to the chosen DEM was selected to initialize SWAT-GL. If a mismatch between DEM and glacier outline acquisition year and mass balance observation start was present, we corrected the initial

285 glacier volume by adding the mass loss or gain that happened since the observation start to the DEM acquisition year. E.g., if mass balance measurements started 1966 and the best DEM and glacier outline was available from 1977, the cumulative mass balance estimates until 1977 were added to the initial volume. The volume was then distributed to the individual ESs while maintaining the original volume fractions of the bands in the total volume. ES sections were defined with a spacing of 100 m. A model run comprised the full available glaciological time series of each catchment, due to differences in the availability of

290 snow cover and the glaciological components. Thus, across glaciers, calibration phases can differ. For example, the glaciers were initialized for the starting year of the mass balance time series (GG 1966, WG 1966, LCG 1953, SCG 1959), while MODIS SC was available from 2002 onward. SC was therefore calibrated from 2002-2015 and validated for the period (2016-2021). For glacier mass balances and glacier hypsometries two calibration phases were used (in contrast to snow cover), one which was the same period as for snow cover (2002-2015) and one at the beginning of the model run (GG 1971-1985, WG

295 1971-1985, SCG 1962-1976, LCG 1953-1967). Discrepancies in the first calibration and validation phase across glaciers stem from different starting dates when measurements started. It was aimed to make use of the full glaciological time series to account for transient behavior in the models. The remainder of the time series was then used as validation phase (one period matching the one of snow cover (2016-2021) and one covering the remaining time series at the end of each glaciers first calibration phase up to 2001). The second validation phase was used in order to make full use of the available information and

300 to assess SWAT-GL over a long time scale. The summary of the temporal settings is given in Table 2. Note that the periods for discharge were intended to match those of the other variables, however, data restrictions did not allow for a perfect match.

2.5.2 Multi-objective Optimization

Although hydrological models traditionally focus on discharge simulation, which is also one of the main goals of SWAT-GL,

305 the glacier routine will be assessed primarily with respect to representing glacier and snow processes. Given the relevance of discharge, the variable will be presented alongside for cross-validation purposes. It is assumed that an adequate discharge

Table 2. Overview of the calibration and validation phases. Note: As discharge was used for cross-validation purposes only, it thus has two validation phases rather than a calibration and validation phase. For the SCG no discharge data was available in the 2000s leading to only one validation period. The asterisk for the WG indicates that validation period II is rather poor due to mainly missing values. For snow cover only one calibration and validation phase was used due to the relatively short temporal coverage of the product, while for glacier variables two calibration and validation periods were used. A minus indicates that a specific second calibration or validation period was not used for this variable.

Glacier	Mass Balance		Snow Cover		Hypsometry		*Discharge*	
	Calibration	Validation	Calibration	Validation	Calibration	Validation	Validation I	Validation II
Gulkana	1971 - 1985	1986 - 2001	2002 - 2015	2016 - 2021	1971 - 1985	1986 - 2001	1971 - 1978	1990 - 2001
	2002 - 2015	2016 - 2021	-	-	2002 - 2015	2016 - 2021	2002 - 2015	2016 - 2021
Lemon Creek	1953 - 1967	1968 - 2001	2002 - 2015	2016 - 2021	1953 - 1967	1968 - 2001	1953 - 1967	1968 - 1973
	2002 - 2015	2016 - 2021	-	-	2002 - 2015	2016 - 2021	2002 - 2015	2016 - 2021
South Cascade	1962 - 1976	1977 - 2001	2002 - 2015	2016 - 2021	1962 - 1976	1977 - 2001	1962 - 1976	1977 - 1992
	2002 - 2015	2016 - 2021	-	-	2002 - 2015	2016 - 2021	-	-
Wolverine	1971 - 1985	1986 - 2001	2002 - 2015	2016 - 2021	1971 - 1985	1986 - 2001	1971 - 1981	1986 - 2001*
	2002 - 2015	2016 - 2021	-	-	2002 - 2015	2016 - 2021	2002 - 2015	2016 - 2021

representation in heavily glacier and snow-dominated catchments could be achieved by a reasonable representation of snow and glacier components. In detail, we calibrated and validated each of the four models based on snow cover (monthly), glacier mass balance variations (annual) and glacier hypsometries (annual) using an automated multi-objective optimization (MOO).

310 As mentioned, discharge simulations (from daily to annual) are provided along to evaluate the model consistency of SWAT-GL. Given the snow- and glacier-focused optimization, only parameters related to SWAT's original snow routine and the newly introduced glacier routine in SWAT-GL were used for the MOO (see Table 3). As a result, 14 parameters were considered in the MOO. We used an automatic MOO procedure, where each of the three prescribed variables referred to one objective (SC, MB, hypsometry). The optimization was performed using the widely used evolutionary NSGA-II (Nondominated Sorting Genetic

315 Algorithm) algorithm (Deb et al., 2002). Based on nondomination sorting and the introduction of a crowding distance operator to favor solutions which are less-crowded (high crowding distance), NSGA-II iteratively finds solutions which are uniformly spread at the Pareto front. The population size of a generation was 100 and the maximum number of generation was set to 100. We used simulated binary cross over with a cross over probability of 0.9 and polynomial mutation with a mutation probability of 0.3.

320 For glacier and snow variables a Normalized Root-Mean-Square Error (f_{NRMSE}), based on the standard deviation of the observations of each variable, was consistently used as objective function (OF) (Eq. 10). The f_{NRMSE} increases comparability between the individual OFs and allows to minimize the residuals between observed and simulated values of all variables. For snow cover we excluded winter months in the optimization procedure to put more weight on the months where snow cover is dynamic as snow cover is usually 100% from December to at least April. The effect is more pronounced in basins with

325 less snow cover dynamics and therefore a relatively high minimum summer snow cover. The simulation of a permanent snow

Table 3. Parameters and their relative ranges used for the benchmarking of SWAT-GL.

Parameter	Description	Minimum	Maximum
SFTMP	Snowfall temperature [°C]	0	4.5
SMTMP	Snowmelt temperature [°C]	0	4.5
SMFMX	Melt factor for snow on June 21 [mm H_2O/(°C·day)]	0.1	7
SMFMN	Melt factor for snow on December 21 [mm H_2O/(°C·day)]	0.1	7
TIMP	Snow temperature lag factor [-]	0	0.5
SNOCOVMX	Snow water equivalent threshold where 100% snow cover occur [mm]	2	75
SNO50COV	Fraction of SNOCOVMX at which 50% snow cover occur [-]	0.1	0.9
TLAPS	Temperature Lapse Rate [°C/km]	-9	-5
PLAPS	Precipitation Lapse Rate [mm/km]	550	1800
GLMLTMP	Threshold temperature for glacier melt [°C]	0	4.5
GLMFMX	Melt factor for ice on June 21 [mm H_2O/(°C·day)]	3.5	13
GLMFMN	Melt factor for ice on December 21 [mm H_2O/(°C·day)]	3.5	10
β_f/f_{frze}	Refreezing factor of glacier melt [-]	0.001	0.01
f_{accu}	Conversion factor of snow to ice [-]	0.1	0.6

cover then leads to good OF values. We will further discuss this issue during the paper. The standard form of the f_{RMSE} can be defined as follows:

$$f_{\text{RMSE,x}} = \sqrt{\frac{\sum_{t=1}^{n}(O_{x,t} - S_{x,t})^2}{n}} \tag{9}$$

with $O_{x,t}$ being observed and $S_{x,t}$ simulated components of variable x, which is either snow cover, glacier mass balance or hypsometry, t refers to the time step (monthly or annual depending on the variable) and n represents the number of available data points. The standardization follows the form:

$$f_{\text{NRMSE,x}} = \frac{f_{\text{RMSE,x}}}{\sigma_x} \tag{10}$$

where σ_x is the standard deviation of the observations of each variable.

However, as glacier hypsometries provide areal time series for multiple glacier elevations, the individual f_{RMSE} of each elevation was calculated and then averaged to obtain one f_{RMSE} value which was standardized in a last step using the standard deviation of observed total glacier area. This gives a more equal weight to all elevations to get rid of solutions where individual elevations might have a high non-standardized error. In other words, if using an average of the f_{NRMSE} of all individual elevations, those with small observed standard deviations (e.g., higher-elevated and less dynamic ones) could lead to an excessive degradation of the overall OF. The f_{PBIAS} is used to show the difference between simulated and observed cumulative mass balance at the end of the simulation period and can be formulated as:

$$f_{\text{PBIAS}} = 100 \cdot \frac{\sum_{t=1}^{n}(S_t - O_t)}{\sum_{t=1}^{n} O_i} \tag{11}$$

with the same declarations as above.

Discharge, used for cross-validation purposes, is based on the Kling Gupta Efficiency (KGE), which is calculated as:

$$f_{\text{KGE}} = 1 - \sqrt{(r-1)^2 + (\alpha-1)^2 + (\beta-1)^2} \tag{12}$$

where r refers to the Pearson Correlation, α to the error in flow variability and β to the bias term with:

$$\alpha = \frac{\sigma_s}{\sigma_o}$$

$$\beta = \frac{\mu_s}{\mu_o}$$

345 with σ and μ referring to the standard deviation and mean of the simulation and observation, respectively.

2.5.3 Statistical Tests

Results for all variables focus on the last generation of the optimization and the best simulations of each variable. Apart from the described methodology, we tested SWAT-GL's ability to reproduce observed mass balance nonstationarities, inter-annual
350 variability and the monotonic relationship between simulated and observed mas balance. For this purpose, the full time series was used, homogeneity was tested with the Wilcoxon-Rank Sum Test (WRS) (Wilcoxon, 1945), the Pettitt Test (Pettitt, 1979) and trends were detected using a modified Mann-Kendall version from Hamed and Ramachandra Rao (1998), which considers autocorrelation. For the WRS the first calibration and the last available validation periods were used. Statistical tests are applied to give an indication whether SWAT-GL is generally able to deal with potential nonstationarities in the catchments, as the model
355 is applied for relatively long simulation periods.

2.5.4 Single-Objective Optimization of SWAT-GL & Benchmarking with SWAT standard

Lastly, for demonstration purposes a Single-Objective Optimization (SOO) was conducted using Differential Evolution (DE) (Storn and Price, 1995) and the adaptations described in Dawar and Ludwig (2014). The SOO demonstration was performed as an example for the WG and two variables, namely mass balance and discharge. For discharge, an additional standard SWAT
360 model without the SWAT-GL glacier extensions was set up for benchmarking purposes taking the benchmarking approach by Seibert et al. (2018) and slightly modified by Merk et al. (2024) as orientation. The standard SWAT model, not considering glaciers adequately, provided a lower benchmark (LB) for the discharge representation using the median value of 1,000 random Latin Hypercube Samples. As upper benchmark (UB) for discharge, again a SOO analogously to the one from SWAT-GL was performed. In summary, the comparison consisted of 5 models for discharge (3 SWAT-GL, 2 SWAT standard) and 3 for mass
365 balance (all SWAT-GL due to the missing components in SWAT standard). An overview is provided in 4
The results of the mass balance SOO model were compared with the results of the MOO introduced previously (covering MB, SC, and hypsometry), while the results of the discharge SOO model were also compared with the LB and UB SWAT models for discharge. The results exemplify how MOO models in glaciated catchments compare to SOO benchmark models for pure

discharge or mass balance calibrations, which is common in hydrological studies. Results therefore demonstrate the impacts of SOO models on general model consistency, missing trade-offs, as well as the structural differences between SWAT and SWAT-GL. Discharge was evaluated based on the f_{KGE} and mass balance again on the f_{NRMSE}. The time periods are equal to those in Table 2. For the SOO of discharge the following additional parameters were included: To account for lags in discharge as well as the general infiltration behavior, SURLAG (surface runoff lag) and CN2 (Curve Number for moisture conditions II) parameters were introduced for the SOO of discharge in contrast to the MOO parameter space of Table 3. The LB and UB models that use SWAT standard share the same parameters and ranges as the discharge SOO model, except for the five glacier parameters available only in SWAT-GL and not in the standard SWAT.

Table 4. Overview of models used for the comparison and evaluation of SWAT-GL.

Model	Calibration Strategy	Optimization Variable	Purpose
SWAT-GL MOO	Multi-Objective Optimization	MB + Hypsometry + SC	Demonstrating glacier representation
SWAT-GL SOO Q	Single-Objective Optimization	Q	Upper benchmark for discharge considering glacier processes
SWAT-GL SOO MB	Single-Objective Optimization	MB	Upper benchmark for mass balance
SWAT UB Q	Single-Objective Optimization	Q	Upper benchmark for discharge not considering glacier processes
SWAT LB Q	Random Sampling	Q	Lower benchmark for discharge not considering glacier processes

3 Results

In the following, the results of the Morris SA and SWAT-GL MOO optimization are presented, complemented by results providing details on the final parameterizations derived from the MOO optimization, results indicating SWAT-GL's representation of inhomogeneities and variability as well as SWAT-GL's representation of discharge. First, the results of the SA are shown (Sect. 3.1), followed by an overview of the final parameter sets across all catchments (Sect. 3.2). Afterwards, the results of SWAT-GL's MOO are illustrated, which represent the main purpose of the paper (Sect. 3.3). The MOO results are supplemented by a short statistical analysis focusing on whether SWAT-GL captures inhomogeneity and variability appropriately (Sect. 3.4), as well as results how the MOO (excluding discharge) is capable of simulating discharge (Sect. 3.5). Lastly, results of two SOO SWAT-GL models that were optimized using discharge and mass balance, respectively, as well as two SWAT standard models serving as LB and UB estimates of discharge, are compared to the MOO results of simulating mass balance, discharge and snow cover (Sect. 3.6).

It is important to note that discharge was excluded from the MOO procedure, as the primary objective of the study is to evaluate SWAT-GL's ability to represent snow and glacier processes. However, given that all catchments are strongly driven by snow and glacier processes, discharge simulations from the MOO are discussed and further compared to a SOO model that solely considers discharge and, therefore, can be seen as an upper benchmark for the discharge representation in these catchments by SWAT-GL.

3.1 SWAT-GL's Glacier and Snow Parameter Sensitivity

The SA is based on the EEs method. Our results for all catchments are presented as scatterplot between μ^*, the mean sensitivity of a factor (parameter), and σ as proxy for the interactions of a factor (Fig. 5).

A common pattern that all catchments share, albeit to varying extents, is their spread around the 1:1 line that differentiates between non-linear and almost-monotonous effects (Garcia Sanchez et al., 2014). Moreover, it is shown that in general the more sensitive parameters (larger μ^*) tend to have higher interactions as well as stronger potential non-linear model responses. It is also shown that the model response of all catchments strongly depends on GLMFMX (blue hexagon) that controls the maximum value of the degree-day factor of ice (and thus the amount of glacier melt that can occur at a specific day of the year). In terms of factor ranking, GLMFMX is the most or the second-most influential factor. It is the most important parameter in the WG & GG basins, where the respective meteorological stations are located directly at the glacier. However, GLMFMX is substituted by the temperature lapse rate (TLAPS, grey circle) at the SCG & LCG, where the respective meteorological stations are located outside of the catchment and at a significant lower elevation than the glaciers. Due to the difference in altitude (which is part of the precipitation correction formulation) between station and elevation band centers it is inherent that the lapse rates become more important. Due to the temperature dominance of both, snow and glacier processes, the sensitivity of the precipitation lapse rate (PLAPS, grey diamond) is less pronounced and strongest at the high-elevated SCG. Among the four most important factors is the threshold temperature of glacier melt (GLMLTMP, blue upward triangle), which controls the onset of melt and has an effect on the timing of melt events as well as the amount of melt. The temperature lapse rate and glacier melt temperature can favor similar conditions or act contradictory (decrease of melt temperature favors earlier melt onset and small or no temperature lapse rate as well). In general, SWAT-GL is strongly temperature-dominated in all catchments.

However, the relevance of precipitation in the SCG basin might be a special characteristic (with regard to the PLAPS ranking in the other basins). In addition, (except for the SCG and LCG) SNOCOVMX (red pentagon) is ranked among the four most sensitive parameters. The parameter determines a threshold of snow water equivalent (SWE) that corresponds to a 100% coverage of snow. As glacier melt can only occur when the glacier is snow-free, the parameter directly affects glacier melt, which explains its relevance in the catchments.

Overall, the ranking shows that across all basins, GLMFMX, TLAPS, GLMLTMP, SNOCOVMX and PLAPS are found to be most often among the most influential parameters.

With respect to potential interactions and non-linear model responses, the accumulation factor (f_accu, blue square) that is responsible for the snow metamorphism (or turnover from snow to ice) takes a dominant role at the WG, GG and SCG. This is plausible as it couples snow and glacier processes by transforming a specific fraction of snow lying on the glacier to ice and thus affecting both storages. Although it is not among the most sensitive factors, it can have a high significance in certain situations due to its possible interactions. Although the most influential parameters receive high σ_{EE} values, they do not necessarily fall in the non-linear area (GG, WG). The strong non-linearity visible for the SCG & LCG might be caused by the fact that the underlying measurement stations are located outside of the catchments at relatively low elevations. All models generally show a non-linear or monotonous behavior and are potentially characterized by interactions rather than a linear relationship.
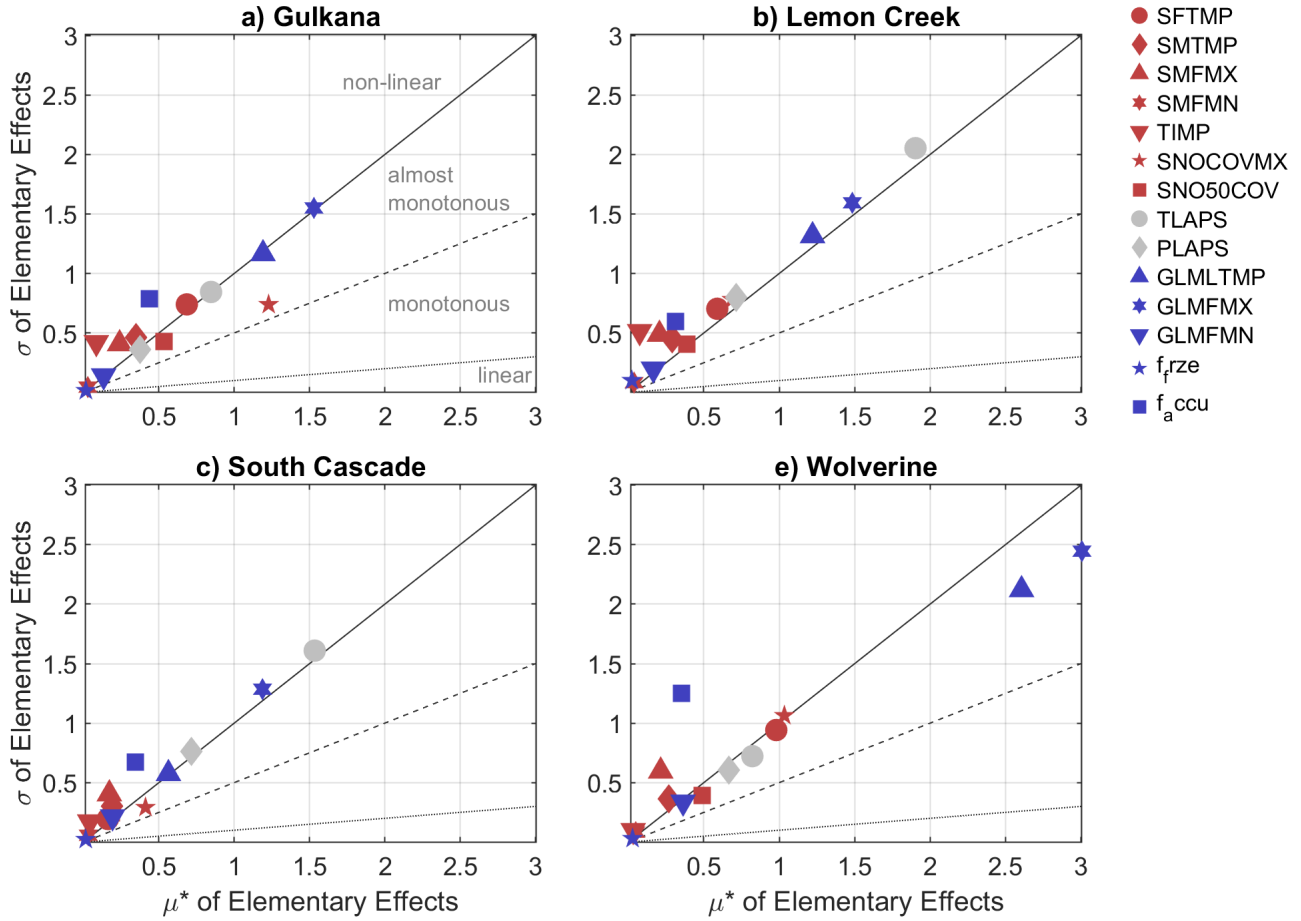
Figure 5. SA results based on the EE method for all four catchments and 14 parameters. The slopes (σ_{EE}/μ^*) of the different lines that classify parameter effects on the model outputs as linear, monotonous, almost monotonous and non-linear are: 0.1 (dotted line), 0.5 (dashed line), 1 (solid line). Red signs refer to snow parameters, gray indicate lapse rates and blue glacier parameters.

Additionally, we identify around 6 to 8 parameters that are less or non-influential, which would reduce the dimensionality of the parameter space for the respective models. However, given the strong interactions of the parameters, the parameter space was kept constant, including the entire space.

3.2 Inter-Basin Comparison of Optimized Glacier Parameters

A comparison between the values of the final parameter sets of all catchments is shown in Fig. 6. As the main purpose is to evaluate the glacier routine introduced in SWAT-GL, the comparison is limited to the five glacier parameters. Results are presented for the f_{NRMSE} values of the annual glacier mass balance only. The parameter values of the GG are relatively well-spaced in the parameter space with an exception for the GLMFMX parameter, which controls the maximum amount of glacier
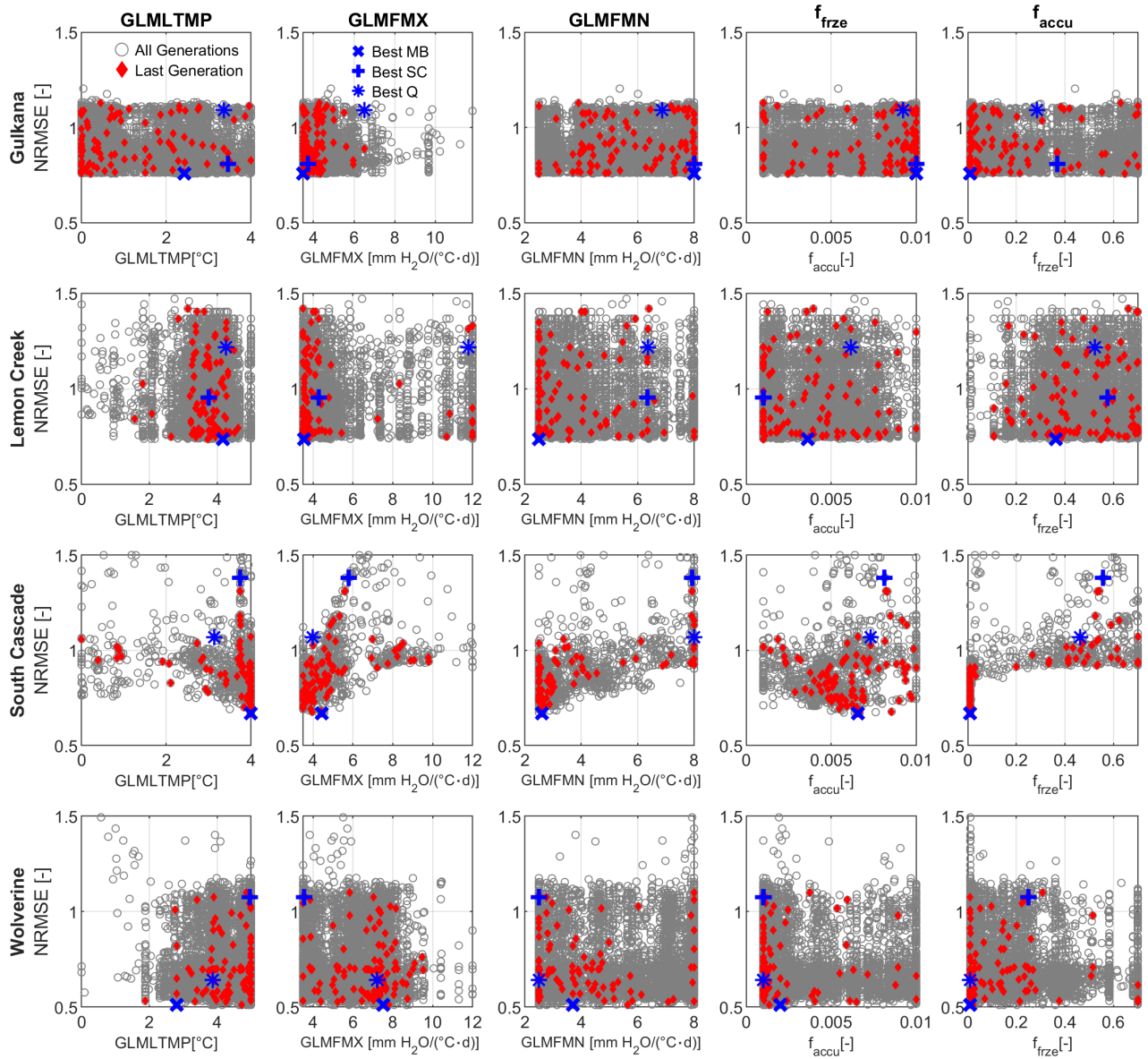
Figure 6. Parameter space illustrated for all glacier-related parameters for all generations (grey) and the final generation (red). The shown f_{NRMSE} values refer to the results of annual glacier mass balance simulations. The three blue symbols refer to the individual best solutions of mass balance, snow cover and (cross-validated) discharge in the last generation. Best hereby means the either the lowest f_{NRMSE} (for SC or MB) or the highest KGE (for discharge) within the last generation.

435 melt. The parameter tends to cluster at its lower boundary for GG, LCG and SCG. The lower bound of GLMFMX is associated with a reduction of strong negative mass balance rates, which might lead to an overestimated ablation. The parameter is among

the most interactive ones, as shown before, indicating that parameter clustering does not necessarily result in a distinct objective function distribution. As Fig. 6 only provides a snapshot for the f_{NRMSE} of MB, the pattern of the objective function space for SC for example could look differently. Analogously to GG, the final parameterizations of the LCG are generally well-spread.

440 An exception exhibits the glacier melt temperature (GLMLTMP) and GLMFMX that both show clustered values. In contrast to the maximum melt factor, the glacier melt threshold temperature groups at its (relatively high) upper bound for the LCG, WG and SCG. The two patterns indicate the necessity of high melt rates, which should not occur too early. The final parameter distribution of the WG is more narrow compared to the other catchments. It is shown that especially for the accumulation rate (f_{accu}), small values are desired to avoid large positive mass balance simulations.

445 Looking at the best parameters for different objectives, it is shown that the best SC simulations can deviate significantly from the best MB simulations (in both the difference in the f_{NRMSE} of the MB and the parameter values). Large deviations in terms of the f_{NRMSE} of the MB can be seen for the SCG and WG (large vertical difference of blue cross and x). With respect to the best final parameters of these two variables, large differences can be observed for GLMLTMP, GLMFMX of the WG (large horizontal distance of blue cross and x), GLMFMN of the SCG and LCG. Moreover, it already becomes apparent that the best

450 discharge simulations do not necessarily coincide with the best simulations of glacier mass balance or snow cover, despite the strong dependency of discharge on snow and glacier melt, which is further discussed in the following chapters.

Table A1 provides a detailed overview of the ranges and median values for each glacier parameter and each catchment at the end of the optimization.

3.3 Evaluating SWAT-GL's Representation of Glacier & Snow Processes

455 The performance of the optimization procedure is shown in Table 5. Statistical results for discharge are presented alongside the other variables for demonstration purposes, although it was not part of the optimization procedure. Results for discharge comprise two validation periods which were chosen analogously to the ones of glacier mass balance, if data was available.

With respect to glacier mass balance estimates, lowest f_{NRMSE} values were found for the WG model (both, calibration and validation), followed by the SCG model. In contrast, the WG model shows the worst performance w.r.t. hypsometries, for

460 which best performance was reached in the GG basin. Concerning snow cover, the LCG and SCG model achieve the best performance metrics in both the calibration and validation period (0.43 and 0.44 for LC model, 0.35 and 0.36 for SC model). Slight variations were observed between the calibration and validation phases for any of the objective functions of all variables included in the optimization procedure. It should be noted that a direct inter-comparison of the absolute f_{NRMSE} values between the catchments is difficult, as the standard deviation of the observations used for the normalization has a dominant effect on the

465 values. For example, the standard deviation of the mass balance observations of the WG is a factor of 1.6 - 9.4 higher than that of the other glaciers (calibration period). The same applies for the snow cover results of the SCG, where observed snow cover standard deviations are 1.3 - 2.4 times above those of the other glaciers.

A clearer picture emerges from the graphical representation of the optimization results in Fig. 7. The discrepancy at the end of the simulation periods of the cumulative mass balance ranges from -1.6% to -55.17%. The relatively large outlier of -

470 55.17% arises from the SCG, where the mass balance loss stagnates in the 1990s. The abrupt change in the mass balance

Table 5. Performance of SWAT-GL for all variables and glaciers with respect to the best simulation of the last generation of the optimization procedure. Numbers in brackets belong to the initial results based on a latin hypercube sampling that serve as starting values for the optimization to provide an indication on the optimization performance. Note: Discharge was not calibrated but is only shown for cross-validation purposes. Discharge thus has two validation phases following the periods assigned to the glacier mass balance evaluation of each glacier (see Sect. 3.3). Cum. B_{gl} refers to the mismatch between observed and simulated cumulative mass balance at the end of the time series and is therefore not attributed to any of the calibration or validation periods. Negative values of Cum. B_{gl} indicate that the model is underestimating mass balance losses. Optimal values for the f_{NRMSE} and f_{PBIAS} are 0 and 1 for the f_{KGE}, respectively.

| Glacier | f_{NRMSE} [-] | | | | | | f_{KGE} | | f_{PBIAS} [%] |
| | Mass Balance | | Snow Cover | | Hypsometry | | Discharge | | Cum. B_{gl} |
	Calibration	Validation	Calibration	Validation	Calibration	Validation	Validation 1	Validation 2	Complete
Gulkana	0.76 (0.80)	0.68	1.08 (1.36)	0.98	0.34 (0.39)	0.28	0.62 (0.71)	0.62	-21.68
Lemon Creek	0.74 (0.86)	0.70	0.43 (0.71)	0.44	0.70 (0.70)	0.75	0.29 (0.32)	0.19	-1.60
South Cascade	0.67 (0.90)	0.69	0.35 (0.46)	0.36	1.13 (1.13)	0.90	0.82 (0.81)	0.59	-55.17
Wolverine	0.51 (0.58)	0.56	0.87 (1.40)	0.99	2.29 (2.30)	1.79	0.64 (0.78)	0.64	-11.16

is also indirectly reflected in the cross-validated results of discharge. While the f_{KGE} in the beginning of the simulation is around 0.82, a significant drop to 0.59 can be observed in the second evaluation period. Problems in the SCG model become especially apparent when focusing on the lower bound of the model range (grey shading in Fig. 7 of cumulative mass balance). Here, we can notice a very poor representation of the inter-annual signal as the simulations show two very abrupt drops and long periods of stagnation. It is likely that the glacier has retreated to altitudes, which are not subject to temperature-induced melting. The wide range visible in the cumulative mass balance could be caused by only a few solutions and does not allow for conclusions about the real distribution of the final simulations. We thus show in Fig. A2 the individual cumulative mass balance representations of all optimized solutions together with the distribution of the cumulative mass balance at the end of the simulation period (all 100 values of the last year of simulation for each glacier). It is found that particularly the upper bound of the GG and WG, as well as the lower bound of the LCG and SCG are caused by a small subset of solutions. The LCG with an almost perfect fit at the end of the simulation period, however, is overestimating ablation for a large part of the simulation period. Overall, the models are underestimating ablation rates after the 2000's (with an exception for the WG). This becomes even more evident by looking at the annual mass balance rates (last column Fig. 7). All models perform well in simulating monthly snow cover, in both, the calibration and validation phase. The spread of the models (grey shading) is relatively large and includes simulations with almost no snow cover in summer. The WG consists of a period of positive mass balance in the 1980s which is likely causing the upward tendency of the simulation range (the share of simulations with a positive cumulative mass balance until the end of the simulation).

Summarizing, the objective function values indicate SWAT-GL being generally capable of representing the glacier dynamics with the exception of the SCG that shows a sharply declining drop in performance over the course of the simulation period. However, a benchmark model would be necessary for an absolute interpretation of the values.
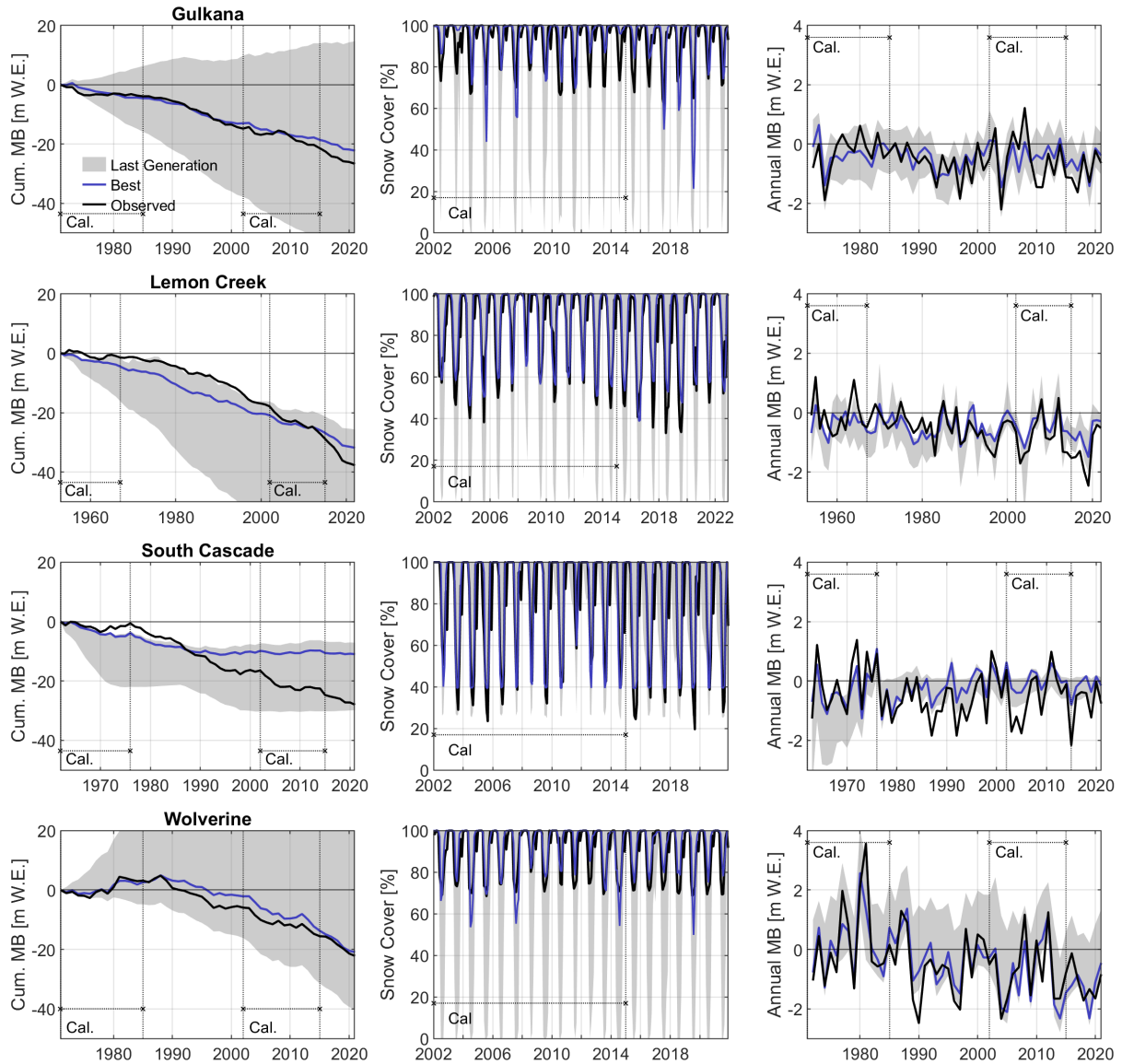
Figure 7. Simulation results of the last generation of the optimization procedure for the cumulative mass balance (Column 1), monthly snow cover (Column 2) and annual mass balance (Column 3). Each row corresponds to one glacier. Blue represents the best evaluation of the last generation for the respective variable, black refers to observations and grey shadings indicate the range of all evaluations part of the last generation. The dashed lines with the Cal. annotation indicates the individual calibration phases of each study area. The remainder of each time series was used for validation.

3.4 SWAT-GL's Ability to Capture Mass Balance Inhomogeneity and Variability

As SWAT-GL was tested for relatively long simulation periods,its capabilities to capture potential inhomogeneities present in the mass balance observations are evaluated. Furthermore, it was investigated how mass balance variability, e.g. represented by the Coefficient of Variation (CV) as proxy for inter-annual variability, are represented by SWAT-GL. Inhomogeneities were determined by a trend detection based on a modified Mann-Kendall and additionally using the Pettitt and Wilcoxon-Rank Sum Test (WRS). The Null Hypothesis of both methods is that the time series contain no change. All results are provided in Table 6. Results of the MK, WRS and Pettitt tests are provided as integers, 0 or 1, indicating whether the null hypothesis was rejected (1) or not (0).

Table 6. Summary of statistical results for the simulated and observed mass balance time series over the whole simulation period. The summary table consists of the Spearman Correlation (ρ), the modified Mann-Kendall after Hamed and Ramachandra Rao (1998) considering autocorrelation (MMK_H), the Sen's Slope estimator, the Coefficient of Variation (CV) as well as the Pettitt and Wilcoxon-Rank Sum (WRS) Test. Results of the MK, WRS and Pettitt tests are provided as integers where 1 indicates the null hypothesis was rejected and 0 that is was accepted.

Glacier	Mass Balance										
	ρ	MK_H		Sen's Slope		CV		Pettitt		WRS	
	-	Sim	Obs	Sim	Obs	Sim	Obs	Sim	Obs	Sim	Obs
Gulkana	0.67	0	1	-5.142e+4	-2.479e+5	1	1.30	0	0	0	1
Lemon Creek	0.62	0	1	-5.846e+4	-2.107e+5	0.88	1.21	0	0	0	0
South Cascade	0.79	1	0	3.281e+4	-1.113e+4	2.75	1.72	1	0	0	0
Wolverine	0.83	1	1	-5.311e+5	-3.931e+5	2.52	2.72	1	1	0	0

While the Spearman Correlation suggests a satisfying to good agreement in the monotonic relationship between simulated and observed mass balance in all catchments, the models failed to represent the trend detection results of the observations. Based on the modified Mann-Kendall test that takes serial correlation into account, SWAT-GL was only in one catchment able to correctly classify the trend statistic. The Sen's slope estimator, used to represent trend magnitudes, differed especially for the outlier SCG model where the sign was mismatched. In the WG and LCG models the simulated trend component was underestimated, while it was overestimated for the WG. The CV, with generally large values mostly above 1, was underestimated in two as well as overestimated in two cases. While it was general in an acceptable range, the SCG again exhibited an outlier. The annual mass balance time series, which were trend-corrected in the presence of a trend, have been further tested on inhomogeneities based on the non-parametric Pettitt and Wilcoxon-Rank Sum Tests.

In summary, the simulations agreed relatively well with the observations at the 0.05 significance level. However, SWAT-GL was not capturing the shift in median detected in the observed time series of the GG (based on the WRS) and additionally rejected the Null Hypothesis of the Pettitt Test for the SCG. However, it can be observed that poor SCG simulations affect the significance of test results.
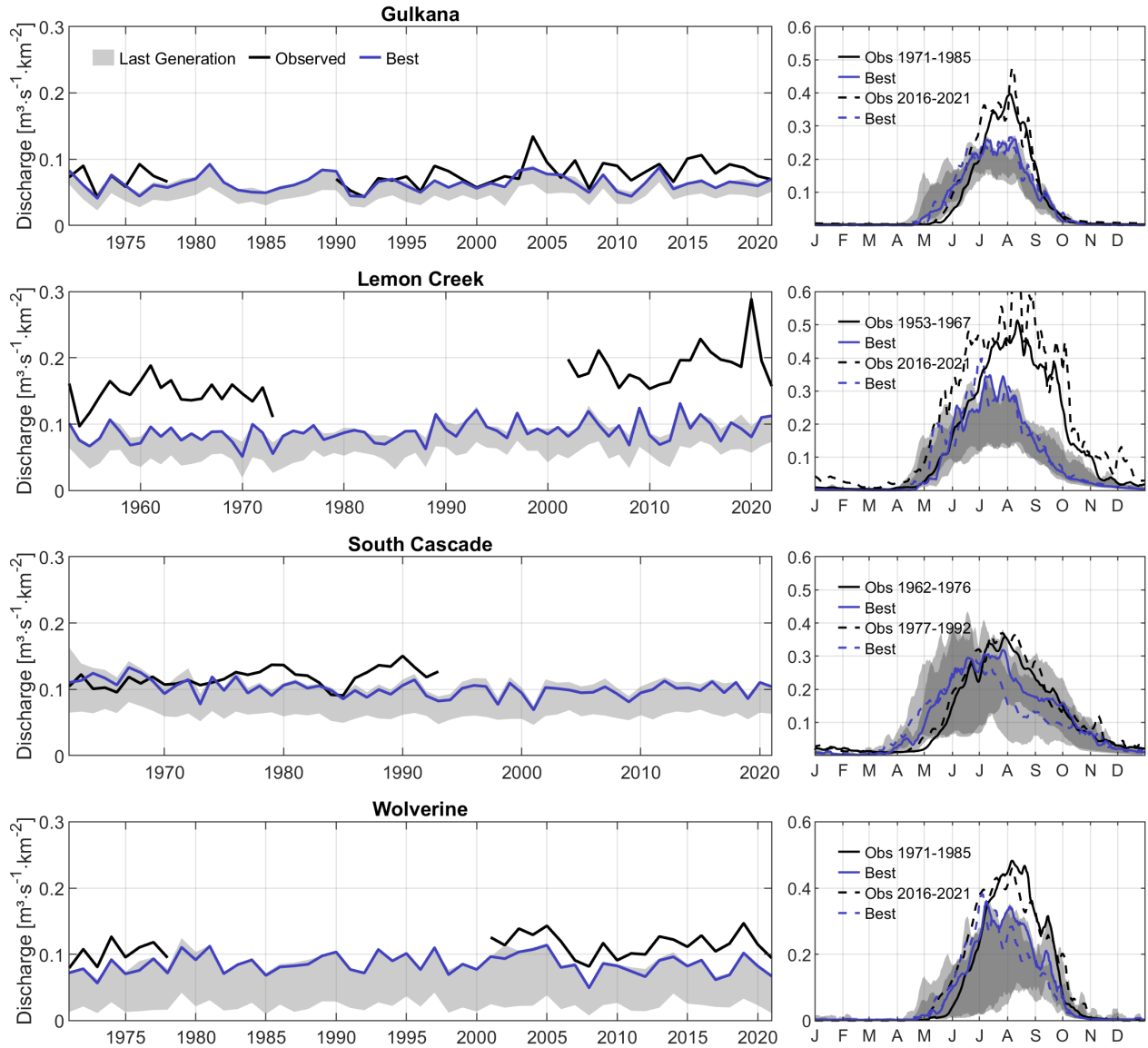
Figure 8. Simulation results for cross-validation of discharge in all four catchments based on mean annual flows (Column 1) and hydrological regimes (Column 2) at the end of the optimization. Hydrological regimes are represented by the mean of daily flows for each day of the year (from day 1 to 366) for the earliest available slice of validation period 1 (solid black line represents observation; solid blue line the best simulation; see also Table 2) and the latest available period of validation period 2 (dashed black line represents observation; dashed blue line the best simulation). Blue lines (simulation) cover the same period as their black counterparts.

3.5 Cross-Validation of Discharge

Discharge in all catchments was cross-validated on the daily scale, assuming that a reasonable fit is achievable, when glacier and snow-related processes are well represented in the heavily glaciated catchments. The performance, evaluated based on the f_{KGE}, can be found in Table 5. The temporal coverage of the validation periods of each catchment is found in Table 2.

First, we see that the GG and WG models show no difference in the f_{KGE} values of the respective validation periods. Second, a significant drop in quality for the SCG model (from validation phase 1 to 2) is found. Lastly, the LCG model acts as a strong outlier with f_{KGE} values <0.3. In contrast, the other three catchments almost entirely show f_{KGE} values >0.6, results often considered satisfactory in hydrological studies according to the classifications of Moriasi et al. (2007); N. Moriasi et al. (2015).

Interestingly, the worst-performing glacier during the glacier-based optimization (SCG) exhibits the best overall discharge performance. Its good quality in the first validation period stems mainly from an overestimated ablation that reduces the underestimation of available water for discharge compared to the other glaciers. Given the large glacier influence in the catchment, the good performance w.r.t. discharge is likely caused for wrong reasons. This stresses the fact that models that are evaluated only for discharge are questionable for comprehensive hydrological investigations. The other glaciers are characterized by a high f_{PBIAS} towards the observations (simulations have less water than observations). The second validation phase of the SCG model, in contrast to the other glaciers, does not cover the 2000s, which are associated with even higher instationarities. Covering the 2000s would likely further reduce the performance metric. f_{PBIAS} is larger in the LCG model, where streamflow is underestimated by 45% and 51% in the calibration and validation phase, respectively.

In addition to the daily performance of Table 5, we further evaluate mean annual flows as illustrated in Fig. 8 together with two separate periods of simulated mean daily discharge (averaged discharge for each day of the year over the indicated periods). For the WG, LCG and GG models a distinct underestimation of annual flows is present in the simulations. When annual flows are centered (mean corrected), a good monotonic relationship for the WG model is observed (see Fig. A3). For the SCG, the deviation of observed and simulated annual discharge increases over time. This further indicates that a temporal coverage of the 2000s of the SCG model would further degrade its results. The annual dynamics of the LCG and GG are only partially met and particularly the larger positive anomalies of the LCG are not captured by the model. Results suggest that inter-annual discharge variability is slightly lower in the model than observed. In general, simulated annual flows of SCG show a decreasing tendency with time, which could be caused by the strong recession initiated at an early stage of the simulation period as shown before (Sect. 3.3). This could then cause a pronounced underestimation of glacier melt contribution especially at end of the simulations as the actually contributing elevations disappeared already.

Evaluating mean daily discharge of the different periods further stresses the substantial undercatch of flow in the simulations (Fig. 8 all glaciers). The periods were chosen so that they lie from each other to highlight potential model deficiencies in the representation of nonstationarities. The LCG and GG models do not show any significant change in the amount of discharge between the early and late period. This points to relatively stable glacier conditions. In contrast, flows in the SCG basin essentially decrease in the later period, which is in line with the aforementioned results. A similar, albeit not as pronounced, pattern is found for the WG model. The model of the SCG shows the largest range of simulated flows over the year (gray shadings).

The share of simulations with a positive mass balance for the WG (see Sect. 3.3) is likely causing the very low simulation bound of discharge in the basin, with almost no flow until August.
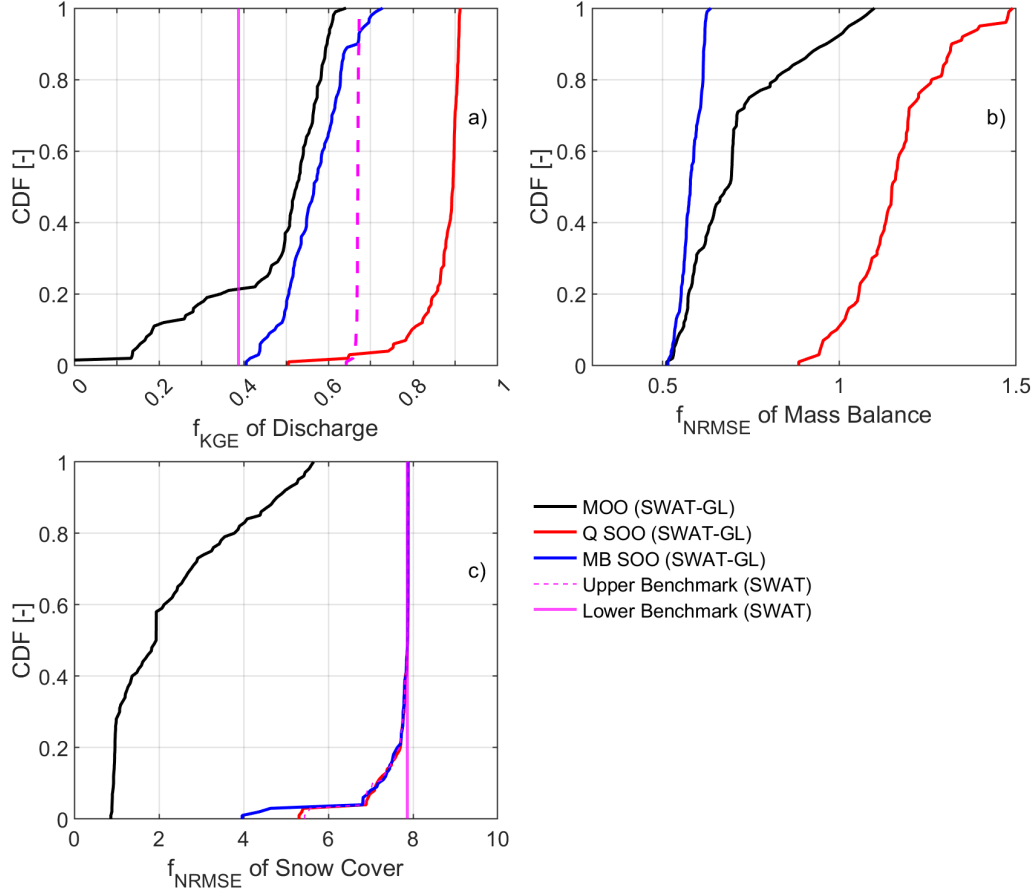
Figure 9. Cumulative distribution function (CDF) plots of the objective functions for the different SWAT-GL models (single-objective optimization (SOO) for mass balance and discharge and multi-objective optimization (MOO)) and the lower benchmark (LB) and upper benchmark (UB) SWAT standard models for the Wolverine Glacier. a) Shows the results for discharge; b) for mass balance (note that no LB and UB are provided as SWAT standard does not simulate mass balance); c) for snow cover. Q SOO refers to the SWAT-GL model optimized for discharge and MB SOO for the SWAT-GL model optimized for mass balance. The CDF of the MOO refer to the last generation (Generation = 100), while the selected SOO results refer to generations to the convergence point where convergence. In detail, the selected generation of the Q SOO and UB model refer to generation 40, and generation 20 for the MB SOO model. The subscripts Q and MB indicate discharge and mass balance, respectively. The sample size N of the CDFs is 100 which refers to the general sample size in the optimization. Note that the LB is a vertical line as it only represents 1 simulation (median f_{KGE} of Q for 1000 latin hypercube samples).

3.6 Comparison of SWAT-GL Single-Objective and Multi-Objective Optimization and SWAT Standard

To illustrate the capabilities of SWAT-GL in terms of discharge and mass balance simulations, two separate SOOs were conducted. The SOO of discharge was evaluated using the f_{KGE} and that of mass balance relied on the f_{NRMSE}, ensuring consistency with the MOO counterpart. Results of the two SOO models are compared with the MOO model results introduced and shown in Sect. 3.3 to 3.5 (using SC, MB and hypsometry). Besides, two SWAT standard models without considering glacier processes were created as lower and upper benchmark models. The LB represents the median f_{KGE} of Q for 1000 latin hypercube-based simulations. The UB model is optimized for discharge only, analogously to the discharge SOO SWAT-GL model. However, it is also based on SWAT rather than SWAT-GL. The evaluation focuses on the WG only and replicates a typical hydrological modeling case where discharge or mass balance only are the only objectives. It is important to note that we are not endorsing this approach as desirable, rather we highlight that, despite well-known shortcomings of SOO studies, the approach remains a common practice. For the SOO of mass balance, parameter choices and ranges are similar to Table 3. The introduction aims to improve SWAT-GL's capabilities in the representation of streamflow.

Results are illustrated in Fig. 9. For discharge (a), the SOO results demonstrate a sharp increase in f_{KGE} values when discharge is used directly as objective, compared to f_{KGE} values from the MOO. The former best f_{KGE} of 0.64 (Table 5) is substituted by a relatively high upper bound of 0.91. The results are reached after 40 generations already and lead to a median f_{KGE} shift from around ~0.5 to around ~0.9. Besides, the median f_{KGE} of the MOO corresponds to the lower bound of the Q SOO. Although the simulated mean annual flow of the MOO procedure showed a significant bias compared to the observed flow (see Fig. 8), the SOO Q results in f_{PBIAS} values of -0.78% (not shown) and is capable of bringing reasonable amounts of water into the system. The MOO shows slightly poorer discharge results compared to those resulting from the MB SOO. Below the 20th percentile the performance of the MOO is largely degraded. The SWAT-based UB model only reaches maximum f_{KGE} values below 0.7 and thus significantly below the Q SOO SWAT-GL counterpart. The LB results is even below 0.4 and even the MOO without Q using SWAT-GL is substantially better (in its median), though worse than the SWAT UB. The highest f_{KGE} values from the MB SOO exceed both, the LB and UB.

The SOO of discharge shows a substantial degradation in representing annual mass balance compared to the MOO and MB SOO (b). The best solution of the SOO of discharge has a f_{NRMSE} value which is ~0.37 above the MOO counterpart (or 78%). Despite a substantially improved MB representation already after 20 generations seen in the MB SOO, the "best" performing simulations (smaller than the 10% percentile) are similar between MOO and MB SOO. The MB SOO model does not exceed the minimum f_{NRMSE} of 0.51 achieved in the MOO, even after convergence. This highlights the suitability of an MOO with SWAT-GL for complex glaciated and snow-fed catchments.

When looking at SC, which was not included in the SOO models but in the MOO, the MOO shows largely superior results. The MB SOO is slightly better in the low percentiles, but generally identical in simulating SC compared to the Q SOO. Also the LB and UB based on SWAT standard show nearly identical results for SC as the two SOO models. It is thus notable how the SC results improve drastically even in a MOO framework compared to simulations where SC is not considered. It would

be interesting whether a SOO using SC only would further improve the results. Furthermore, the comparability, especially for discharge, is constrained since it was not considered in the MOO.

4 Discussion & Outlook

As a profound evaluation of SWAT-GL's performance in different glaciated catchments was missing so far, the intention was to contribute to close this gap with our work. Note that further information with respect to technical details of SWAT-GL and future plans about model improvements are found in Schaffhauser et al. (2024).

4.1 Glacier Parameterizations & Process Representation

We used the Method of Morris to identify (screen) and rank glacier and snow parameters in the four basins (Song et al., 2015; Pianosi et al., 2016; Sarrazin et al., 2016).

In general, lapse rates together with parameters controlling the maximum degree-day factor for ice (and thus glacier melt) were shown to be among the most sensitive parameters in all catchments. The strong temperature-dependence of SWAT-GL is further emphasized by the high sensitivity of the threshold temperature when glacier melt occurs. An important role plays the SWE threshold that determines when a (sub-)basin is fully snow-covered. The parameter links the old snow routine and the newly integrated glacier routine, as glacier melt can only occur under snow-free conditions on the glacier. SWAT's snow cover received growing attention in multi-objective calibration studies that try to improve model consistency (Tuo et al., 2018; Grusson et al., 2015). The fraction of snow cover is directly affecting the amount of daily snow melt (lower fractions reduce the amount of snow melt) and indirectly glacier melt. As any degree of snow cover can be achieved with any SWE, there is also the risk to accomplish good snow cover results with implausible amounts of snow. This circumstance is, contradictory to its importance, rarely discussed in the literature. SWE measurements can therefore add significant benefits as they provide valuable insights on actual amounts of snow. However, resolutions of reanalysis or remote sensing-based SWE products, along with the significant variability observed in product comparison studies, remain a challenge. SWE observations would be more suitable for drawing conclusions about precipitation inputs compared to relying solely on snow cover. We want to further emphasize that the intermediate sensitivity of precipitation lapse rates might be misleading. The objectives chosen might not be valid to allow for precipitation-related conclusions as none of the three variables is based on absolute volumes (of snow or ice). For example, a separate consideration of summer ablation and winter accumulation would provide a more realistic picture of system in- and outputs.

As SWAT-GL is still in its early stages, the SA was conducted for diagnostic purposes, involving screening and ranking among different catchments. This was done independently of the optimization purpose. In future applications, the dimensions of the parameter space should be reduced accordingly. The SA for example suggested a reduction of the parameter space (by 6-8 dimensions) in the different catchments of the study. The derived glacier parameter sets after optimization, are relatively well-spread in the parameter space. However, in the demonstration catchments, the maximum melt factor tends to group at its defined lower bound. This indicates a potential reduction of the lower bound for an even better representation of glacier

mass balance. The chosen values could be reduced, however, as SWAT-GL internally makes a plausibility check between the estimated snow and ice degree-day factors, a further reduction might make internal corrections of the degree-day factor more likely. In addition, further reducing the lower bound of the parameter might exacerbate the strong underestimation of flow. The high values of the glacier melt temperature imply that the models seem to compensate for other temperature-dependent processes as the model seems to try to delay glacier melt. This indicates that glaciers are, despite the good SC representation, snow free and exposed to melting too early. A lag factor similar to the temperature lag factor of snow already present in SWAT could also give further control in the timing of glacier melt. However, our study has shown that the snow lag factor is not very sensitive, although its lower bound was chosen to avoid abrupt and extreme snow melt events. We further propose that alternative solutions concerning the lag of ice and snow melt might be explored and evaluated in order to decouple them more clearly from the lag factor related to effective precipitation.

Overall, the standard deviation of the Elementary Effects indicate that glacier and snow processes behave strongly non-linear and exhibit potential interacting effects, which we see as a further indication of SWAT-GL's suitability. The moderate interaction ability for SNOCOVMX is considered to be unusual, as it links snow and glacier processes which would suggest higher interaction and/or non-linearity. Future work might put attention on Time-Varying Sensitivity Analysis (TVSA), such as DYNIA or also using EEs, to obtain further insights in parameter dominance at different scales and periods over time (Chiogna et al., 2024). Especially in the context of climate impact assessment, insights of a potential loss in model skill due to a reduction in the dominance of (historically working) parameter sets in non-stationary systems become crucial (Wagener, 2022).

4.2 SWAT-GL's Performance in Representing Glaciated Catchments

The optimization procedure using NSGA-II for snow cover, glacier hypsometry and glacier mass balance worked well for the highly glaciated catchments with the exception of the SCG. For the SCG, an abrupt change in the mass balance estimates in the middle of the simulation period causes implausible results. However, snow cover estimates were very good in all catchments and we highly recommend to use snow cover as an objective function for an adequate representation of mountain hydrology when using SWAT-GL. This is particularly true as MODIS (or other) snow cover data is relatively easy to access and widely available, unlike glacier mass balance measurements, which are more challenging to obtain. In data-scarce regions, predominantly the typical setting of high-mountainous areas, snow cover in combination with downstream measured discharge might often be the only sources of data for calibration and validation.

While annual net mass balance was well represented, it was noticed that glacier melt tends to start too early leading to an extended overlapping period where snow and glacier melt contribute equally to runoff generation. The mass balance estimates are better represented for the bigger glaciers or catchments respectively. However, SWAT-GL was introduced to provide a simple but efficient approach to represent glacier dynamics on multiple scales. While SWAT applications often focus on larger scales compared to the relatively small SCG, more evaluation is necessary on the reasons for the bad performance and whether it might be linked to the small spatial scale. Something which is especially important to investigate given the overall trend of shrinking glaciers across the world.

As hypsometry measurements were available, they were used in the optimization process. In future work total glacier area

might be a suitable alternative to the individual hypsometry time series. As the Δh-parameterization assumes upper parts of a glacier to be more stable we conclude that the approach might fail to represent the dynamics of the upper elevation sections at the SCG and LCG while it seems more appropriate for the WG and GG (see Fig. A4). Using total area changes could therefore improve the representation of the overall MOO, as it would circumvent the attempt to reproduce a pattern SWAT-GL is structurally not able to. Similarly, if individual hypsometry time series are used one might consider to put less weight on the upper parts of the glacier.

We have shown that, by using discharge as a single-objective, as done for the WG, the performance could be substantially ameliorated (f_{KGE} >0.9). Using mass balance in the SOO (again for WG), we have shown that the best solutions of the MOO were comparable to those resulting from the SOO with respect to the achieved f_{NRMSE} values. The statistical results of the mass balance estimates significantly dropped using discharge for SOO and could not compete with the MOO mass balance results. In contrast, the discharge performance as a result from the mass balance SOO was better than the discharge representation of the MOO. Unlike mass balance, discharge was not part of the MOO objectives and partly constrains the interpretability. The benchmarking of the discharge optimized SWAT-GL model against SWAT standard illustrated the importance of adequate structural representations in high mountain environments. In addition, the results indicate the limited applicability of SWAT standard in glaciated catchments even when solely conditioned on discharge.

However, the difficulty in achieving model consistency in highly glaciated and mountainous basins became particularly visible in the LC basin. The studied glaciers generally have a high contribution to streamflow, as for example found in O'Neel et al. (2014) (for GG and WG). Since we consistently overestimate ablation for the LCG, it is initially contradictory that we obtain streamflow underestimations of up to about 50% (ablation mainly referred to glacier melt). Potential reasons can be manifold. A wrong representation of snow amounts and distribution, despite a good snow cover fit, or an underestimation of liquid precipitation (or a combination of the two) might be potential reasons. Moreover, similarly to what is described in O'Neel et al. (2014), the model could also underestimate summer ablation and winter accumulation which govern the mass balance, which would again be related to precipitation. However, it seems that precipitation input might be too low since the LCG meteorological data stems from a remote valley station and the model relies on optimized lapse rates. Precipitation estimates in mountainous catchments can generally be considered as a complex field coming with large uncertainties that are then reflected in our hydrological models (Evin et al., 2024). Therefore future modeling work could also try to not only use net mass balance but (if available) make further use of seasonal mass balance (winter accumulation & summer ablation) derivations in the calibration strategy (Schaefli and Huss, 2011). The winter mass balances could also be used to additionally validate the precipitation inputs from the stations and to adjust the precipitation laps rates.

In general, it became evident that SWAT-GL has great capabilities to be applied in glaciated catchments, also for longer, non-stationary time scales. It is assumed that the simple degree-day approach integrated in the mass balance module alone could cause significant improvements in glaciated catchments. The simplicity of the approach also leads to high transferability with manageable effort.

4.3 Glacier Initialization

A further very sensitive factor that affects the simulation results, in particular under long simulation periods which are likely subject to persistent climate change effects, is the initialization of the glacier mass. Datasets such as from Farinotti et al. (2019) or Millan et al. (2022) provide valuable information on glacier thickness and thus mass initialization. But attention should be paid when simulation periods start decades ago before the considered thickness estimates. A comparison of the mass differences between the Farinotti estimates and our own calculations based on GlabTop-2 for the earliest possible DEM and outline (see Sect. 2.5) reveal substantial differences. The magnitudes are between -11% to +19%. The contradictory signs are produced as the Randolph Glacier Inventory outlines for the different glaciers stem from different acquisition years which are sometimes earlier than the outlines used for GlabTop-2. This emphasizes the importance of the initialization assumptions. In greater detail, temperature conditions back then might not be suitable to trigger glacier melt in an appropriate magnitude as lower glacier bounds are simply located too high. Basically, there would be a mismatch between the link of glacier elevation and runoff generation. This becomes evident when examining areal losses as fraction of initial area of each glacier over the simulation period (see Appendix A5), where fractional area losses range from more than 10% (WG) to more than 40% (SCG). The Δh approach implemented in SWAT-GL does not consider glacier flow and does allow for glacier area growth (not be confused with accumulation in ice water equivalent of a specific ES) in its current version, which is relevant especially for long simulation periods with phases of growth.

5 Conclusions

The recently extended version of SWAT, called SWAT-GL, was tested in representing the hydrology of four highly glaciated basins. The new SWAT-GL, which makes use of a physically-based glacier evolution routine has proven to provide robust hydrological simulations of catchments that are characterized by nivo-glacial processes. It thus serves its purpose and adds a valuable contribution to the hydrological modeling community, and in particular, the SWAT community.

We also identified traditional model consistency issues prevalent in hydrological modeling and demonstrated their significance, even when multiple glacier and snow processes are included in the calibration procedure. Although SWAT-GL substantially improves model consistency, such problems should receive more attention. Although we could show SWAT-GL's applicability even under long transient conditions, constraints remain and require further efforts to address. This is particularly true for climate impact studies, where simulation periods can exceed 100 years. In such studies, we advocate a minimum requirement that assesses the suitability of model components for climate impact statements to avoid flawed conclusions. Transient conditions, for example, could significantly affect degree-day factors, making initial choices inappropriate. A topic that is rarely addressed and discussed.

We identified parameter clustering at the edges of the initial parameter ranges, which indicate solutions that could impair physical plausibility. In addition, contradictory patterns were found in the representation of snow and glacier processes (and discharge). For example, a good representation of the snow and glacier processes partly resulted in an unsatisfactory representation of streamflow. We demonstrated that an adequate to good snow cover simulation does not necessarily lead to an accurate

representation of glacier components. These basic insights, although partly recognized, go beyond SWAT-GL applications and are of general importance for the modeling community. The sensitivity analysis of SWAT-GL emerged a strong temperature-dependence of the model. This underpinned the importance and role of lapse rate parameterizations, also as a major source of uncertainty, in high mountain catchments. However, by benchmarking different SWAT-GL models against SWAT standard, substantial improvements in representing water availability were highlighted.

Despite SWAT-GL was tested in catchments that are unprecedented in terms of data availability, the authors see no restrictions in its transferability to areas with poor data. Global datasets of ice thickness estimates and glacier outline set a suitable baseline to apply SWAT-GL. Although relatively small glaciated catchments were employed, the approach can be scaled up without imposing any substantial additional computational demand or physical limitation on the approach.

In conclusion, the most significant merit we discovered with SWAT-GL was its ability to adequately represent glacier processes and outperforming SWAT standard in contrasting glaciated catchments. This encourages its further application and need in high-mountain catchments.

Code and data availability. Code and executable of SWAT-GL can be acquired from https://gitlab.com/lshm1/swat-g. The underlying hydrological, meteorological and glaciological data can be obtained from the USGS benchmark glacier project:https://www.usgs.gov/publications/us-geological-survey-benchmark-glacier-project

Appendix A
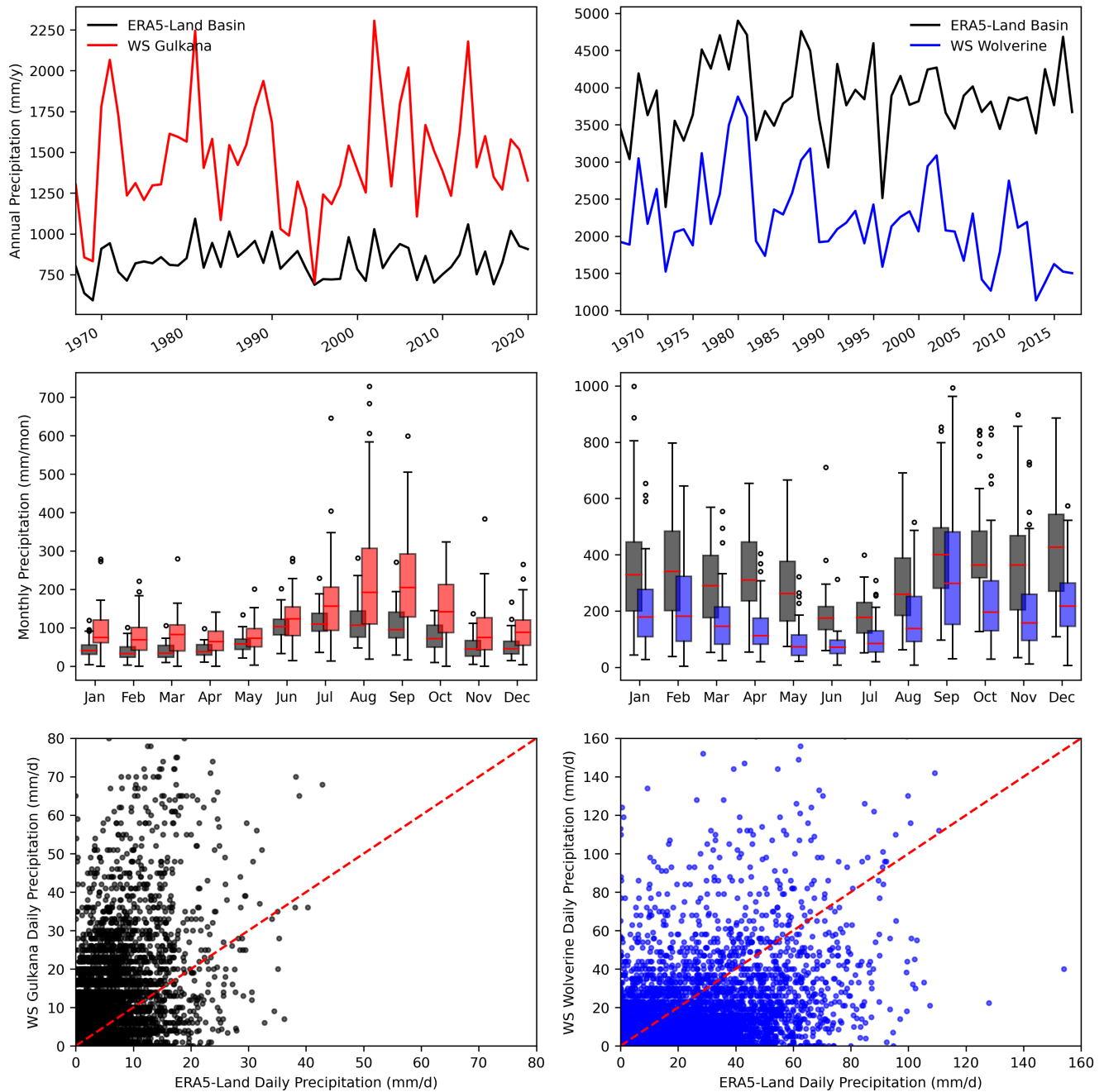
Figure A1. Comparison of the used Weather Station (WS) precipitation data with ERA-Land Reanalysis data for the Wolverine and Gulkana glaciers, as the station data refers to local stations. ERA5-Land results refer to the mean over all pixels that touch the corresponding basin boundary (4 pixels for both basins).
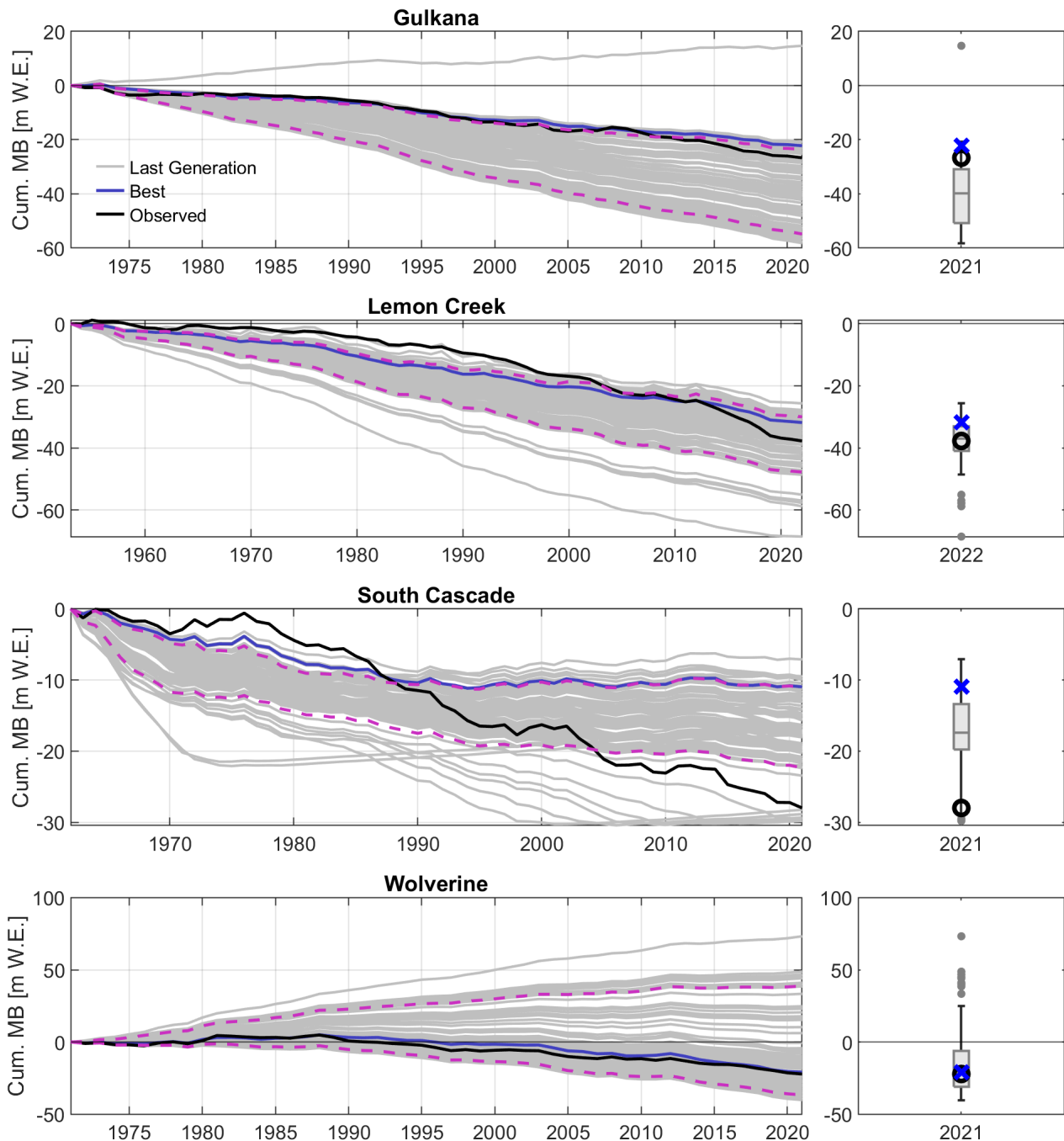
Figure A2. Similar to cumulative mass balance plot of Fig. 7 but providing all individual solutions of the final generation instead of the range. The boxplots provide an estimate of the distribution of the cumulative mass balance at the end of simulation period. For example the boxplot of GG consists of the 100 individual cumulative mass balance estimates of year 2021. Blue crosses indicate the results of the best annual mass balance representation in the optimization and black circle indicate the final observed value. Dashed purple lines refer to the 10th and 90th percentiles.
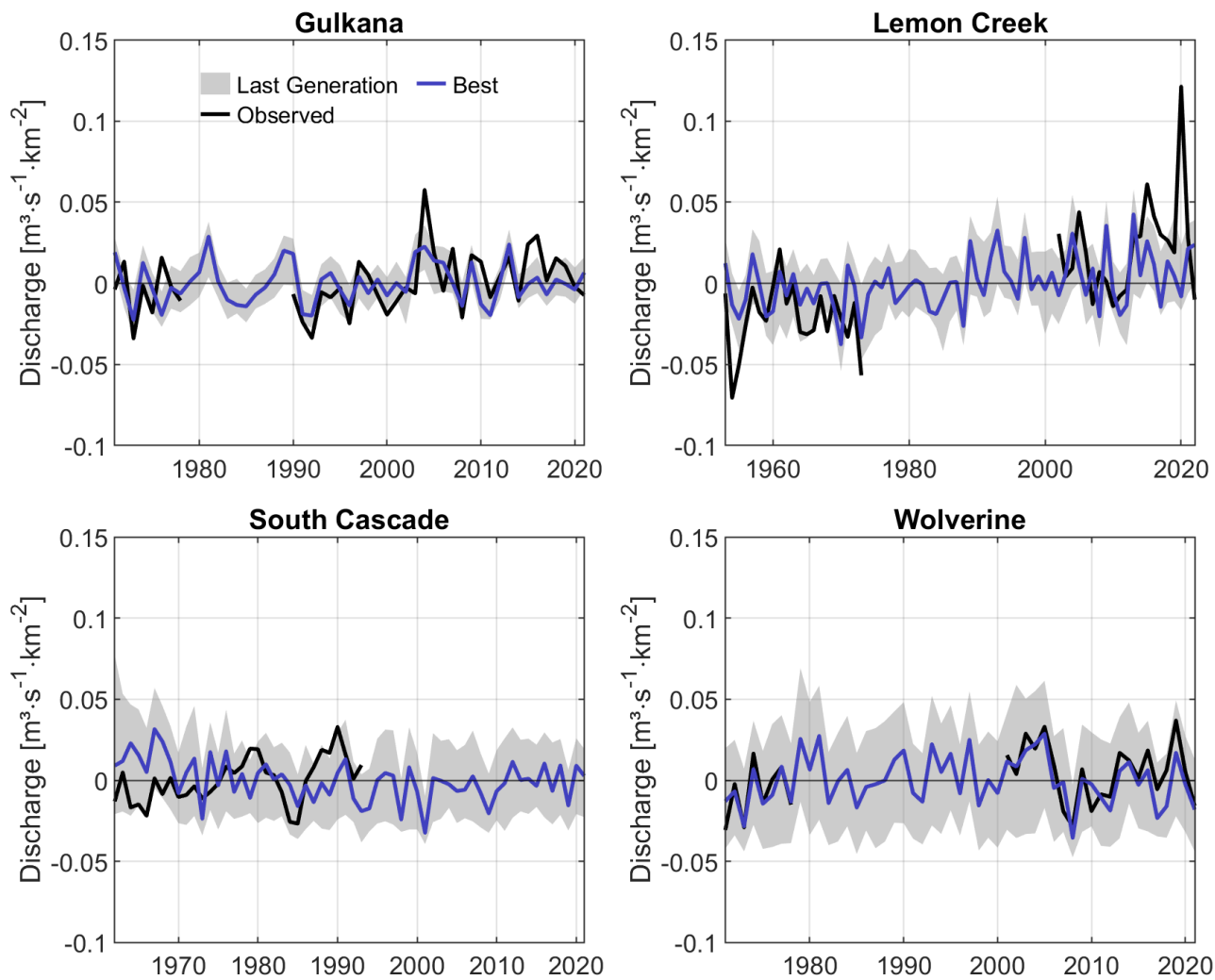
Figure A3. Simulation results for centered specific mean annual discharge.
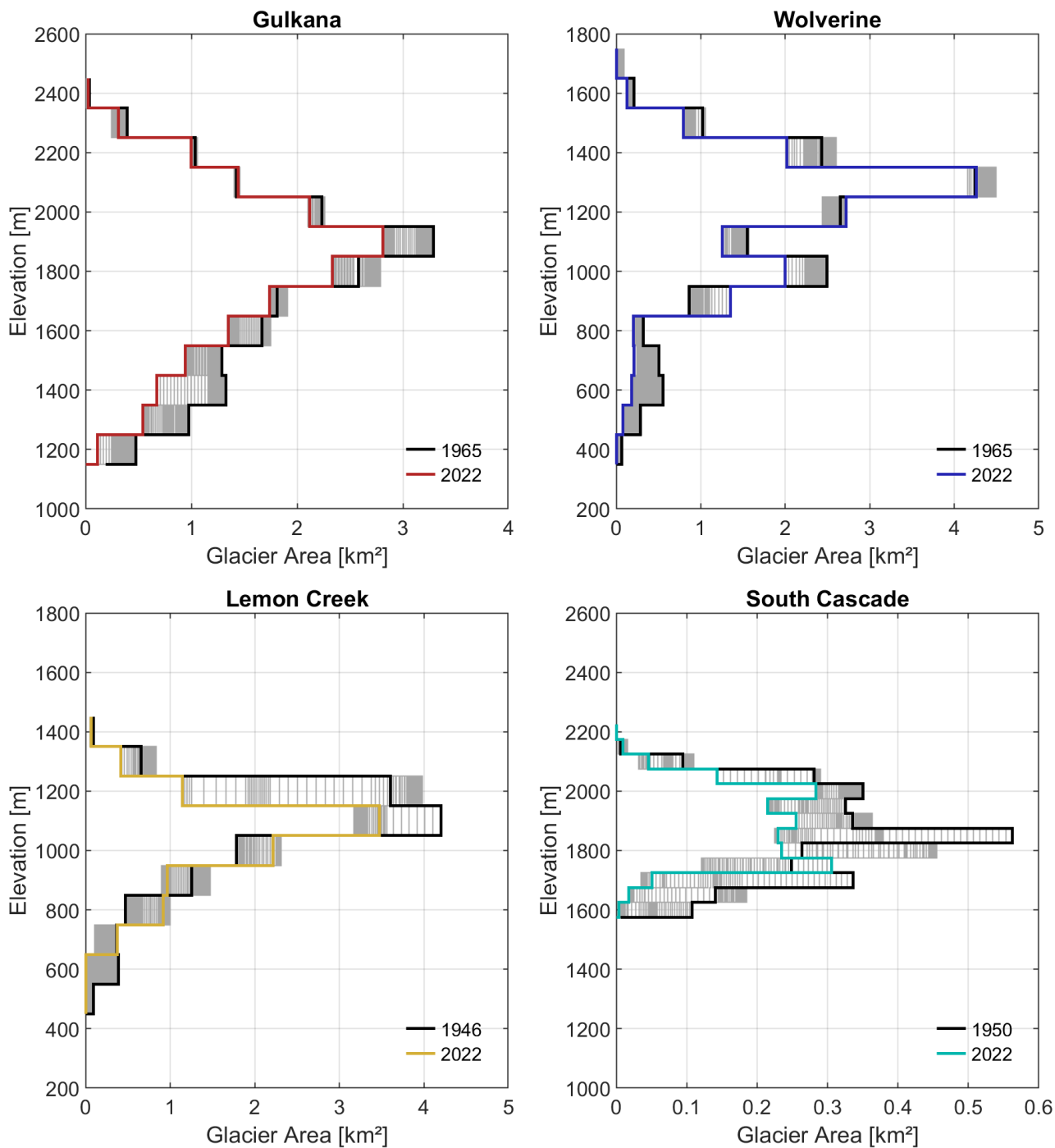
Figure A4. Annual glacier hypsometry observations for all four glaciers. Grey indicates each year where data was available while black represents the first available year and the individual colors the last available year of measurements.
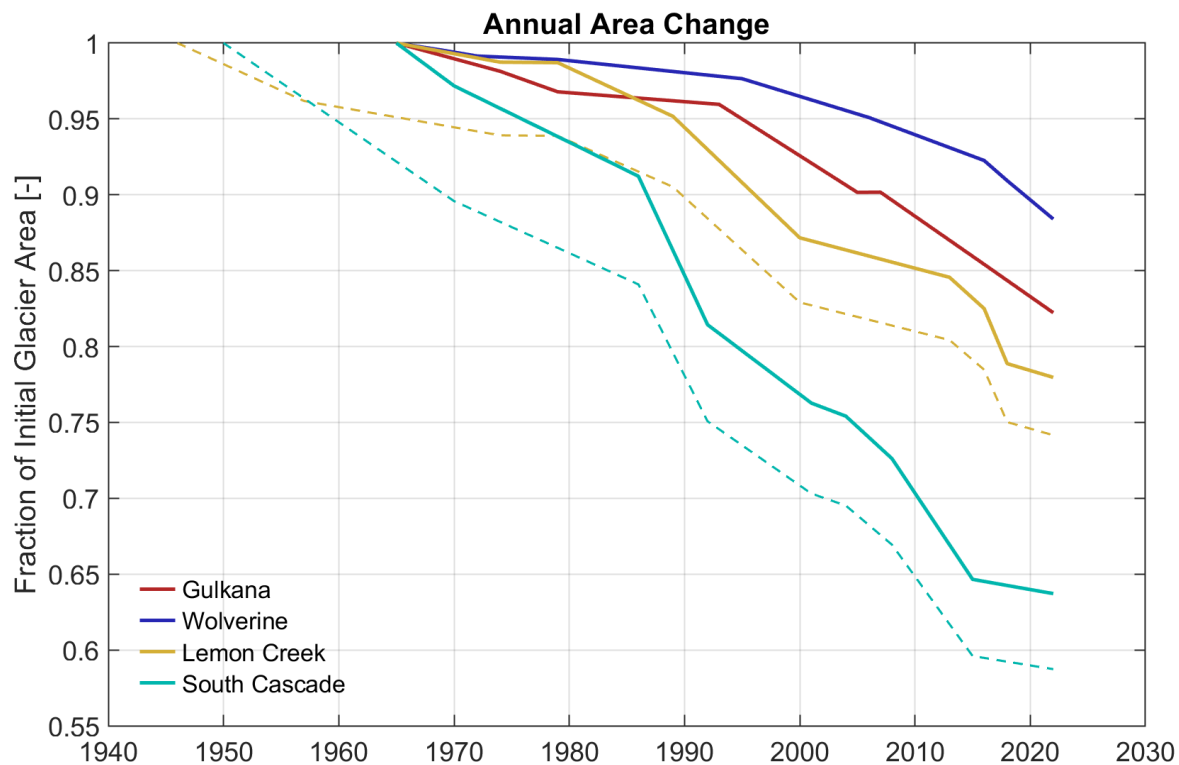
Figure A5. Observed annual glacier area observations of all glaciers expressed as fraction of initial area. Solid lines represent the earliest date of overlap between all glaciers and dashed lines represent the dates at which the mass balance measurement start in case it deviates from the starting point of the solid counterpart (only the case for SCG and LCG).

Table A1. Parameter ranges and median values of all glaciers for the last generation of the optimization. Note: only the glacier parameters are shown here, which is the main novelty and purpose of the article.

Glacier	GLMLTMP			GLMFMX			GLMFMN			f_{frze}			f_{accu}		
	Min	Max	Median	Min	Max	Median	Min	Max	Median	Min	Max	Median	Min	Max	Median
GG	0	4.00	0.70	3.50	6.51	4.05	2.50	8.00	5.76	0.001	0.01	0.0092	0.01	0.70	0.09
LCG	1.56	4.62	3.75	3.50	12.00	3.70	2.50	8.00	2.95	0.001	0.01	0.0033	0.01	0.70	0.45
SCG	0	4.00	3.92	3.50	12.00	4.40	2.50	8.00	2.74	0.001	0.01	0.0059	0.01	0.70	0.01
WG	1.88	5.00	4.49	3.50	9.53	7.13	2.50	8.00	3.30	0.001	0.01	0.001	0.01	0.70	0.03

Author contributions. TS, FM, FH, GC, MD, YT, LA, JM manuscript review and editing; TS, FM, MD study design; TS, FM, JM data acquisition; TS, FM, FH, JM data analysis and modeling; TS, FM, FH, GC, MD, YT, LA, JM model evaluation. TS manuscript draft.

730

Competing interests. The contact author has declared that none of the authors has any competing interests.

Acknowledgements. We gratefully acknowledge support from the United States Geological Survey (USGS) Benchmark Glacier Project for providing the comprehensive datasets. This work was supported by the EU Horizon Europe project WE-ACT (ID: 101083481). The authors also want to thank Scott Boyce from USGS for assisting the work.

735 **References**

Adnan, M., Kang, S., Zhang, G., Saifullah, M., Anjum, M. N., and Ali, A. F.: Simulation and Analysis of the Water Balance of the Nam Co
Lake Using SWAT Model, Water, 11, 1383, https://doi.org/10.3390/w11071383, 2019.

Ali, S. H., Bano, I., Kayastha, R. B., and Shrestha, A.: COMPARATIVE ASSESSMENT OF RUNOFF AND ITS COMPONENTS
IN TWO CATCHMENTS OF UPPER INDUS BASIN BY USING A SEMI DISTRIBUTED GLACIO-HYDROLOGICAL MODEL,
740 The International Archives of the Photogrammetry, Remote Sensing and Spatial Information Sciences, XLII-2/W7, 1487–1494,
https://doi.org/10.5194/isprs-archives-xlii-2-w7-1487-2017, 2017.

Arnold, J. G., Srinivasan, R., Muttiah, R. S., and Williams, J. R.: LARGE AREA HYDROLOGIC MODELING AND ASSESSMENT
PART I: MODEL DEVELOPMENT, Journal of the American Water Resources Association, 34, 73–89, https://doi.org/10.1111/j.1752-
1688.1998.tb05961.x, 1998.

745 Bahr, D. B., Pfeffer, W. T., and Kaser, G.: A review of volume-area scaling of glaciers, Reviews of Geophysics, 53, 95–140,
https://doi.org/10.1002/2014rg000470, 2015.

Baker, E. H., Mcneil, C. J., Sass, L., Peitzsch, E. H., Whorton, E. N., Florentine, C. E., Clark, A. M., Miller, Z. S., Fagre, D. B., and O'Neel,
S. R.: USGS Benchmark Glacier Mass Balance and Project Data, https://doi.org/10.5066/F7BG2N8R, 2018.

Campolongo, F., Saltelli, A., and Cariboni, J.: From screening to quantitative sensitivity analysis. A unified approach, Computer Physics
750 Communications, 182, 978–988, https://doi.org/10.1016/j.cpc.2010.12.039, 2011.

Chen, Y., Li, W., Fang, G., and Li, Z.: Review article: Hydrological modeling in glacierized catchments of central Asia – status and challenges,
Hydrology and Earth System Sciences, 21, 669–684, https://doi.org/10.5194/hess-21-669-2017, 2017.

Chiogna, G., Marcolini, G., Engel, M., and Wohlmuth, B.: Sensitivity analysis in the wavelet domain: a comparison study, Stochastic Envi-
ronmental Research and Risk Assessment, https://doi.org/10.1007/s00477-023-02654-3, 2024.

755 Copernicus Climate Change Service: ERA5-Land hourly data from 2001 to present, https://doi.org/10.24381/CDS.E2161BAC, 2019.

Dawar, D. and Ludwig, S.: Differential evolution with dither and annealed scale factor, in: 2014 IEEE Symposium on Differential Evolution
(SDE), IEEE, https://doi.org/10.1109/sde.2014.7031528, 2014.

Deb, K., Pratap, A., Agarwal, S., and Meyarivan, T.: A fast and elitist multiobjective genetic algorithm: NSGA-II, IEEE Transactions on
Evolutionary Computation, 6, 182–197, https://doi.org/10.1109/4235.996017, 2002.

760 Dozier, J.: Spectral signature of alpine snow cover from the landsat thematic mapper, Remote Sensing of Environment, 28, 9–22,
https://doi.org/https://doi.org/10.1016/0034-4257(89)90101-6, 1989.

Du, X., Silwal, G., and Faramarzi, M.: Investigating the impacts of glacier melt on stream temperature in a cold-region watershed: Coupling
a glacier melt model with a hydrological model, Journal of Hydrology, 605, 127 303, https://doi.org/10.1016/j.jhydrol.2021.127303, 2022.

Evin, G., Le Lay, M., Fouchier, C., Penot, D., Colleoni, F., Mas, A., Garambois, P.-A., and Laurantin, O.: Evaluation of hydrological
765 models on small mountainous catchments: impact of the meteorological forcings, Hydrology and Earth System Sciences, 28, 261–281,
https://doi.org/10.5194/hess-28-261-2024, 2024.

Farinotti, D., Huss, M., Fürst, J. J., Landmann, J., Machguth, H., Maussion, F., and Pandit, A.: A consensus estimate for the ice thickness
distribution of all glaciers on Earth, Nature Geoscience, 12, 168–173, https://doi.org/10.1038/s41561-019-0300-3, 2019.

Frey, H., Machguth, H., Huss, M., Huggel, C., Bajracharya, S., Bolch, T., Kulkarni, A., Linsbauer, A., Salzmann, N., and Stoffel,
770 M.: Estimating the volume of glaciers in the Himalayan–Karakoram region using different methods, The Cryosphere, 8, 2313–2333,
https://doi.org/10.5194/tc-8-2313-2014, 2014.

Gan, R., Luo, Y., Zuo, Q., and Sun, L.: Effects of projected climate change on the glacier and runoff generation in the Naryn River Basin, Central Asia, Journal of Hydrology, 523, 240–251, https://doi.org/10.1016/j.jhydrol.2015.01.057, 2015.

Garcia Sanchez, D., Lacarrière, B., Musy, M., and Bourges, B.: Application of sensitivity analysis in building energy simulations: Combining first- and second-order elementary effects methods, Energy and Buildings, 68, 741–750, https://doi.org/10.1016/j.enbuild.2012.08.048, 2014.

Grusson, Y., Sun, X., Gascoin, S., Sauvage, S., Raghavan, S., Anctil, F., and Sáchez-Pérez, J.-M.: Assessing the capability of the SWAT model to simulate snow, snow melt and streamflow dynamics over an alpine watershed, Journal of Hydrology, 531, 574–588, https://doi.org/10.1016/j.jhydrol.2015.10.070, 2015.

Hamed, K. H. and Ramachandra Rao, A.: A modified Mann-Kendall trend test for autocorrelated data, Journal of Hydrology, 204, 182–196, https://doi.org/10.1016/s0022-1694(97)00125-x, 1998.

Hassan, J., qing Chen, X., Kayastha, R. B., and Nie, Y.: Multi-model assessment of glacio-hydrological changes in central Karakoram, Pakistan, Journal of Mountain Science, 18, 1995–2011, https://doi.org/10.1007/s11629-021-6748-9, 2021.

Hofmeister, F., Arias-Rodriguez, L. F., Premier, V., Marin, C., Notarnicola, C., Disse, M., and Chiogna, G.: Intercomparison of Sentinel-2 and modelled snow cover maps in a high-elevation Alpine catchment, Journal of Hydrology X, 15, 100 123, https://doi.org/10.1016/j.hydroa.2022.100123, 2022.

Horlings, A.: A Numerical Modeling Investigation on Calving and the Recession of South Cascade Glacier, Tech. rep., https://doi.org/10.15760/honors.307, 2016.

Huss, M. and Hock, R.: A new model for global glacier change and sea-level rise, Frontiers in Earth Science, 3, https://doi.org/10.3389/feart.2015.00054, 2015.

Huss, M., Farinotti, D., Bauder, A., and Funk, M.: Modelling runoff from highly glacierized alpine drainage basins in a changing climate, Hydrological Processes, 22, 3888–3902, https://doi.org/10.1002/hyp.7055, 2008.

Huss, M., Jouvet, G., Farinotti, D., and Bauder, A.: Future high-mountain hydrology: a new parameterization of glacier retreat, Hydrology and Earth System Sciences, 14, 815–829, https://doi.org/10.5194/hess-14-815-2010, 2010.

Ji, H., Fang, G., Yang, J., and Chen, Y.: Multi-Objective Calibration of a Distributed Hydrological Model in a Highly Glacierized Watershed in Central Asia, Water, 11, 554, https://doi.org/10.3390/w11030554, 2019.

Li, H., Beldring, S., Xu, C.-Y., Huss, M., Melvold, K., and Jain, S. K.: Integrating a glacier retreat model into a hydrological model – Case studies of three glacierised catchments in Norway and Himalayan region, Journal of Hydrology, 527, 656–667, https://doi.org/10.1016/j.jhydrol.2015.05.017, 2015.

Linsbauer, A., Paul, F., and Haeberli, W.: Modeling glacier thickness distribution and bed topography over entire mountain ranges with GlabTop: Application of a fast and robust approach, Journal of Geophysical Research: Earth Surface, 117, n/a–n/a, https://doi.org/10.1029/2011jf002313, 2012.

Linsbauer, A, Paul, F, Hoelzle, M, Frey, H, and Haeberli, W: The Swiss Alps without glaciers – a GIS-based modelling approach for reconstruction of glacier beds, https://doi.org/10.5167/UZH-27834, 2009.

Luo, Y., Arnold, J., Liu, S., Wang, X., and Chen, X.: Inclusion of glacier processes for distributed hydrological modeling at basin scale with application to a watershed in Tianshan Mountains, northwest China, Journal of Hydrology, 477, 72–85, https://doi.org/10.1016/j.jhydrol.2012.11.005, 2013.

Luo, Y., Wang, X., Piao, S., Sun, L., Ciais, P., Zhang, Y., Ma, C., Gan, R., and He, C.: Contrasting streamflow regimes induced by melting glaciers across the Tien Shan – Pamir – North Karakoram, Scientific Reports, 8, https://doi.org/10.1038/s41598-018-34829-2, 2018.

810 Ma, C., Sun, L., Liu, S., Shao, M., and Luo, Y.: Impact of climate change on the streamflow in the glacierized Chu River Basin, Central Asia, Journal of Arid Land, 7, 501–513, https://doi.org/10.1007/s40333-015-0041-0, 2015.

Mcneil, C. J., Sass, L., Florentine, C., Baker, E. H., Peitzsch, E. H., Whorton, E. N., Miller, Z., Fagre, D. B., Clark, A. M., and O'Neel, S. R.: Glacier-Wide Mass Balance and Compiled Data Inputs: USGS Benchmark Glaciers, https://doi.org/10.5066/F7HD7SRF, 2016.

Merchán-Rivera, P., Geist, A., Disse, M., Huang, J., and Chiogna, G.: A Bayesian framework to assess and create risk maps of groundwater
815   flooding, Journal of Hydrology, 610, 127 797, https://doi.org/10.1016/j.jhydrol.2022.127797, 2022.

Merk, F., Schaffhauser, T., Anwar, F., Tuo, Y., Cohard, J.-M., and Disse, M.: The significance of the leaf area index for evapotranspiration estimation in SWAT-T for characteristic land cover types of West Africa, Hydrology and Earth System Sciences, 28, 5511–5539, https://doi.org/10.5194/hess-28-5511-2024, 2024.

Millan, R., Mouginot, J., Rabatel, A., and Morlighem, M.: Ice velocity and thickness of the world's glaciers, Nature Geoscience, 15, 124–129,
820   https://doi.org/10.1038/s41561-021-00885-z, 2022.

Moriasi, D. N., Arnold, J. G., Liew, M. W. V., Bingner, R. L., Harmel, R. D., and Veith, T. L.: Model Evaluation Guidelines for Systematic Quantification of Accuracy in Watershed Simulations, Transactions of the ASABE, 50, 885–900, https://doi.org/10.13031/2013.23153, 2007.

Morris, M. D.: Factorial Sampling Plans for Preliminary Computational Experiments, Technometrics, 33, 161–174,
825   https://doi.org/10.1080/00401706.1991.10484804, 1991.

N. Moriasi, D., W. Gitau, M., Pai, N., and Daggupati, P.: Hydrologic and Water Quality Models: Performance Measures and Evaluation Criteria, Transactions of the ASABE, 58, 1763–1785, https://elibrary.asabe.org/abstract.asp?aid=46548&t=3, 2015.

NASA JPL: NASA Shuttle Radar Topography Mission Global 1 arc second, https://doi.org/10.5067/MEASURES/SRTM/SRTMGL1.003, 2013.

830 Naz, B. S., Frans, C. D., Clarke, G. K. C., Burns, P., and Lettenmaier, D. P.: Modeling the effect of glacier recession on streamflow response using a coupled glacio-hydrological model, Hydrology and Earth System Sciences, 18, 787–802, https://doi.org/10.5194/hess-18-787-2014, 2014.

Nossent, J., Elsen, P., and Bauwens, W.: Sobol' sensitivity analysis of a complex environmental model, Environmental Modelling Software, 26, 1515–1525, https://doi.org/https://doi.org/10.1016/j.envsoft.2011.08.010, 2011.

835 O'Neel, S., Hood, E., Arendt, A., and Sass, L.: Assessing streamflow sensitivity to variations in glacier mass balance, Climatic Change, 123, 329–341, https://doi.org/10.1007/s10584-013-1042-7, 2014.

O'Neel, S., McNeil, C., Sass, L. C., Florentine, C., Baker, E. H., Peitzsch, E., McGrath, D., Fountain, A. G., and Fagre, D.: Reanalysis of the US Geological Survey Benchmark Glaciers: long-term insight into climate forcing of glacier mass balance, Journal of Glaciology, 65, 850–866, https://doi.org/10.1017/jog.2019.66, 2019.

840 Pesci, M. H., Schulte Overberg, P., Bosshard, T., and Förster, K.: From global glacier modeling to catchment hydrology: bridging the gap with the WaSiM-OGGM coupling scheme, Frontiers in Water, 5, https://doi.org/10.3389/frwa.2023.1296344, 2023.

Pettitt, A. N.: A Non-Parametric Approach to the Change-Point Problem, Applied Statistics, 28, 126, https://doi.org/10.2307/2346729, 1979.

Pianosi, F., Beven, K., Freer, J., Hall, J. W., Rougier, J., Stephenson, D. B., and Wagener, T.: Sensitivity analysis of environmental models: A systematic review with practical workflow, Environmental Modelling & Software, 79, 214–232,
845   https://doi.org/10.1016/j.envsoft.2016.02.008, 2016.

Pradhananga, N. S., Kayastha, R. B., Bhattarai, B. C., Adhikari, T. R., Pradhan, S. C., Devkota, L. P., Shrestha, A. B., and Mool, P. K.: Estimation of discharge from Langtang River basin, Rasuwa, Nepal, using a glacio-hydrological model, Annals of Glaciology, 55, 223–230, https://doi.org/10.3189/2014aog66a123, 2014.

RGI Consortium: Randolph Glacier Inventory - A Dataset of Global Glacier Outlines, Version 6, https://doi.org/10.7265/4M1F-GD79, 2017.

850 Saltelli, A., Ratto, M., Andres, T., Campolongo, F., Cariboni, J., Gatelli, D., Saisana, M., and Tarantola, S.: Global sensitivity analysis: the primer, John Wiley & Sons, 2008.

Sarrazin, F., Pianosi, F., and Wagener, T.: Global Sensitivity Analysis of environmental models: Convergence and validation, Environmental Modelling & Software, 79, 135–152, https://doi.org/10.1016/j.envsoft.2016.02.005, 2016.

Schaefli, B. and Huss, M.: Integrating point glacier mass balance observations into hydrologic model identification, Hydrology and Earth
855 System Sciences, 15, 1227–1241, https://doi.org/10.5194/hess-15-1227-2011, 2011.

Schaffhauser, T., Tuo, Y., Hofmeister, F., Chiogna, G., Huang, J., Merk, F., and Disse, M.: SWAT-GL: A new glacier routine for the hydrological model SWAT, JAWRA Journal of the American Water Resources Association, https://doi.org/10.1111/1752-1688.13199, 2024.

Seibert, J., Vis, M. J. P., Kohn, I., Weiler, M., and Stahl, K.: Technical note: Representing glacier geometry changes in a semi-distributed hydrological model, Hydrology and Earth System Sciences, 22, 2211–2224, https://doi.org/10.5194/hess-22-2211-2018, 2018.

860 Shafeeque, M., Luo, Y., Wang, X., and Sun, L.: Altitudinal Distribution of Meltwater and Its Effects on Glacio-Hydrology in Glacierized Catchments, Central Asia, JAWRA Journal of the American Water Resources Association, 56, 30–52, https://doi.org/10.1111/1752-1688.12805, 2019.

Shannon, S. R., Payne, A., Freer, J., Coxon, G., Kauzlaric, M., Kriegel, D., and Harrison, S.: A snow and glacier hydrological model for large catchments – case study for the Naryn River, Central Asia, https://doi.org/10.5194/hess-2022-51, 2022.

865 Sin, G. and Gernaey, K. V.: Improving the Morris method for sensitivity analysis by scaling the elementary effects, in: Computer Aided Chemical Engineering, pp. 925–930, Elsevier, https://doi.org/10.1016/s1570-7946(09)70154-3, 2009.

Song, X., Zhang, J., Zhan, C., Xuan, Y., Ye, M., and Xu, C.: Global sensitivity analysis in hydrological modeling: Review of concepts, methods, theoretical framework, and applications, Journal of Hydrology, 523, 739–757, https://doi.org/10.1016/j.jhydrol.2015.02.013, 2015.

870 Stoll, E., Hanzer, F., Oesterle, F., Nemec, J., Schöber, J., Huttenlau, M., and Förster, K.: What Can We Learn from Comparing Glacio-Hydrological Models?, Atmosphere, 11, 981, https://doi.org/10.3390/atmos11090981, 2020.

Storn, R. and Price, K.: Differential Evolution: A Simple and Efficient Adaptive Scheme for Global Optimization Over Continuous Spaces, Journal of Global Optimization, 23, 1995.

Tebaldi, C., Debeire, K., Eyring, V., Fischer, E., Fyfe, J., Friedlingstein, P., Knutti, R., Lowe, J., O'Neill, B., Sanderson, B., van Vuuren, D.,
875 Riahi, K., Meinshausen, M., Nicholls, Z., Tokarska, K. B., Hurtt, G., Kriegler, E., Lamarque, J.-F., Meehl, G., Moss, R., Bauer, S. E., Boucher, O., Brovkin, V., Byun, Y.-H., Dix, M., Gualdi, S., Guo, H., John, J. G., Kharin, S., Kim, Y., Koshiro, T., Ma, L., Olivié, D., Panickal, S., Qiao, F., Rong, X., Rosenbloom, N., Schupfner, M., Séférian, R., Sellar, A., Semmler, T., Shi, X., Song, Z., Steger, C., Stouffer, R., Swart, N., Tachiiri, K., Tang, Q., Tatebe, H., Voldoire, A., Volodin, E., Wyser, K., Xin, X., Yang, S., Yu, Y., and Ziehn, T.: Climate model projections from the Scenario Model Intercomparison Project (ScenarioMIP) of CMIP6, Earth System Dynamics, 12,
880 253–293, https://doi.org/10.5194/esd-12-253-2021, 2021.

Tiel, M., Stahl, K., Freudiger, D., and Seibert, J.: Glacio-hydrological model calibration and evaluation, WIREs Water, 7, https://doi.org/10.1002/wat2.1483, 2020.

Tuo, Y., Duan, Z., Disse, M., and Chiogna, G.: Evaluation of precipitation input for SWAT modeling in Alpine catchment: A case study in the Adige river basin (Italy), Science of The Total Environment, 573, 66–82, https://doi.org/10.1016/j.scitotenv.2016.08.034, 2016.

885 Tuo, Y., Marcolini, G., Disse, M., and Chiogna, G.: A multi-objective approach to improve SWAT model calibration in alpine catchments, Journal of Hydrology, 559, 347–360, https://doi.org/10.1016/j.jhydrol.2018.02.055, 2018.

U.S. Geological Survey: USGS Water Data for the Nation, https://doi.org/10.5066/F7P55KJN, 1994.

Vanuytrecht, E., Raes, D., and Willems, P.: Global sensitivity analysis of yield output from the water productivity model, Environmental Modelling Software, 51, 323–332, https://doi.org/https://doi.org/10.1016/j.envsoft.2013.10.017, 2014.

890 Wagener, T.: On the Evaluation of Climate Change Impact Models for Adaptation Decisions, p. 33–40, Springer International Publishing, https://doi.org/10.1007/978-3-030-86211-4_5, 2022.

Wang, X., Zhang, Y., Luo, Y., Sun, L., and Shafeeque, M.: Combined use of volume-area and volume-length scaling relationships in glacio-hydrological simulation, Hydrology Research, 49, 1753–1772, https://doi.org/10.2166/nh.2018.137, 2018.

Wiersma, P., Aerts, J., Zekollari, H., Hrachowitz, M., Drost, N., Huss, M., Sutanudjaja, E. H., and Hut, R.: Coupling a global glacier
895 model to a global hydrological model prevents underestimation of glacier runoff, Hydrology and Earth System Sciences, 26, 5971–5986, https://doi.org/10.5194/hess-26-5971-2022, 2022.

Wilcoxon, F.: Individual Comparisons by Ranking Methods, Biometrics Bulletin, 1, 80, https://doi.org/10.2307/3001968, 1945.

Wortmann, M., Bolch, T., Krysanova, V., and Buda, S.: Bridging glacier and river catchment scales: an efficient representation of glacier dynamics in a hydrological model, https://doi.org/10.5194/hess-2016-272, 2016.

900 Wu, F., Zhan, J., Wang, Z., and Zhang, Q.: Streamflow variation due to glacier melting and climate change in upstream Heihe River Basin, Northwest China, Physics and Chemistry of the Earth, Parts A/B/C, 79-82, 11–19, https://doi.org/10.1016/j.pce.2014.08.002, 2015.

Yang, C., Xu, M., Fu, C., Kang, S., and Luo, Y.: The Coupling of Glacier Melt Module in SWAT Model Based on Multi-Source Remote Sensing Data: A Case Study in the Upper Yarkant River Basin, Remote Sensing, 14, 6080, https://doi.org/10.3390/rs14236080, 2022.

Zekollari, H., Huss, M., Farinotti, D., and Lhermitte, S.: Ice-Dynamical Glacier Evolution Modeling—A Review, Reviews of Geophysics,
905 60, https://doi.org/10.1029/2021rg000754, 2022.